Pore-Scale Simulations of Unsteady Flow and Heat Transfer in Tubular Fixed Beds

P. Magnico
Laboratoire de Génie des Procédés Catalytiques, CNRS-ESCPE Lyon, 43 bd du 11 Novembre 1918, B.P. 2077, 69616 Villeurbanne Cedex, France

DOI 10.1002/aic.11806
Published online March 11, 2009 in Wiley InterScience (www.interscience.wiley.com).

Small tube-to-particle-diameter ratio induces a radial heterogeneity in tubular fixed beds on the particle scale. In this complex topology, theoretical models fail to predict wall-to-fluid heat transfer. In order to be more realistic, a deterministic Bennett method is first used to synthesize two packings with a tube-to-sphere-diameter ratio of 5.96 and 7.8, containing 236 and 620 spheres, respectively. In a second step, unsteady velocity and temperature fields are computed by CFD. In the range of Reynolds number lying between 80 and 160, hydrodynamic results are validated with experimental data. The thermal disequilibrium in the near-wall region is described in detail. Several pseudo-homogeneous models are compared to the numerical simulations. The radial and axial profiles of temperature show a clear agreement with the model of Schlünder's research group and the model of Martin and Nilles. © 2009 American Institute of Chemical Engineers *AIChE J*, 55: 849–867, 2009

Keywords: fixed bed, computational fluid dynamics, unsteady flow, flow maldistribution, heat transfer

Introduction

Tubular fixed beds are used in many processes like absorbers, chemical reactors, and heat exchangers. The study of heat transfer is of the utmost importance with regard to yield, stability, selectivity, and catalytic deactivation. In the presence of highly exothermic or endothermic heterogeneous gas-solid reactions, the radial heat transfer (through the packed bed and at the wall) is increased by using a small tube-to-particle diameter ratio. Therefore, accurate correlation for the effective transverse thermal conductivity and for the wall heat-transfer coefficient at the wall is necessary. Until several decades ago, much experimental work and models were devoted to the determination of correlations. However, the analysis of the experimental data was carried out by means of very simplistic models which assume that the fixed bed is a homogeneous effective porous medium. This leads to the assumption of parameters, such as porosity, permeability; heat conductivity constant in space.[1–3] Moreover, the heat conductivity of the two phases, as well as their wall heat-transfer coefficient is combined in one parameter. The other main approximation is the presence of a temperature jump at the reactor wall. This assumption cannot be used at small and moderate Reynolds numbers. Owing to these simplistic assumptions, the standard two-parameter model gives a wide scatter of the Nusselt number and the radial conductivity.[4]

In the case of a tube-to-particle diameter ratio smaller than 10, the wall of the fixed bed induces a radial heterogeneity of the compacity. The consequence of this is the presence of a fluid flow maldistribution, and a radial gradient of the thermal conductivity especially close to the reactor wall. Therefore, the global parameters mentioned previously must be used locally because of their dependence upon the local compacity.[5–8] Some attempts have been made to take into account the heterogeneity in the standard model by using a radial profile of velocity computed with a Brinkman-Forchheimer phenomenological equation or a radial profile of the effective thermal conductivity. This approach, however, must be used carefully. Even if the two phases are taken

P. Magnico's e-mail address is pmo@lobivia.cpe.fr.

into account, there is no distinction on the microscopic scale. Experimental investigations show that the scale of the heterogeneity is of the order of the particle diameter, i.e., lower than the Darcy scale, although the two phases are clearly separated at this scale. Consequently, in order to match the Brinkman-Forchheimer equation with their experimental velocity data, Giese et al,[9] Bey and Eigenberger,[10] and also Givler and Altobelli,[11] used an effective turbulent viscosity, which can tend to a value greater than one as the Reynolds number decreases to zero. Despite those improvements, the published correlations do not correctly predict the magnitude and the longitudinal position of the hot spot in the presence of an exothermic chemical reaction even in turbulent regime.[12–13]

The spatial heterogeneity is in fact composed of two contributions: the radial heterogeneity and the spatial separation of the two phases. If we consider the hydrodynamic aspect, the phase separation induces a transversal contribution of the convective heat and mass transfer. It also induces a strong coupling in space of the three velocity components. The time correlation has also to be taken into account according to the hydrodynamic regime. Another approach, which is more rigorous, consists in computing at the pore scale the velocity and the temperature field. This approach needs to build the packing in order to compute the velocity field between the particles, and the heat and mass transfer in the two phases by CFD. The main interest of this is to introduce the topologic heterogeneity in a realistic way, and to describe its influence on the heat transfer on the local scale. The other advantage is to avoid the use of the heat transfer limitation at the reactor tube wall. For many years, this method of investigation was performed at low Reynolds numbers for hydrogeological applications:[14–16] permeability computation, transport properties, dissolution and clogging mechanism, etc. For a few years, the microscopic approach is used in the case of a tubular fixed bed, but most of the packed beds are structured and/or contained only few grains.[17–22] Only a few numerical results from representative fixed-bed reactors are available in the literature.[23–27] The published numerical studies on heat transfer are mainly carried out by means of the standard turbulence models which assume that the turbulence is well established, i.e., a Reynolds number range much greater than 200. Owing to the complexity of the topology, the turbulence is not homogeneous and isotropic. Therefore, the turbulent parameters such as the viscosity and the heat conductivity are unknown.

In this work, we present numerical results on the heat transfer properties of fixed beds in the range of Reynolds number lower than 160. The hydrodynamics and the temperature field are computed by means of the resolution of the standard 3-D (three-dimensional) Navier-Stokes equations and the laminar heat-transfer equation. The unsteady equations must be solved because in this range of Reynolds number the laminar flow is unstable. The direct numerical simulation has the advantage of minimizing the number of hypotheses contrary to turbulent models: no-slip conditions, prescribed temperature at the inlet and at the reactor wall. On the other hand, the disadvantage of the DNS is the limited Reynolds number range due to the computational requirement (small grid size and time step). In this work, the diameter ratio d_t/d_p is 5.96 and 7.8, respectively. In order to use representative fixed beds, the computational domains contain several hundred spheres. The fluid is assumed to be a gas whose physical properties are independent of the temperature. From these results the CFD approach will be compared to several standard macroscopic models.

Microscopic Approach

Packing simulations

The 3-D computation first requires the fixed-bed structure to be represented. The geometrical structure may be analyzed by tomography or magnetic resonance imaging. In this case the generated packing mimics the sample exactly and the numerical results (velocity or concentration) can be compared locally with *in situ* measurement data.[23,25] The numerical approach is also often used.[19,21,24,27] Among many methods, the Bennet technique is used in this work. This approach consists in adding sequentially new spheres one at a time on a basal horizontal plane. The choice of the site of deposition used in the literature is also varied.[28] In order to obtain a packing stable under gravity, the added sphere, is, therefore, in contact with three other ones already in place if the sphere is not in contact with the horizontal plane. Other contacts, like one sphere in contact with two or four spheres, are not taken into account. Spheres are generally added in a cubic container with a lateral periodic boundary condition i.e., in the absence of a vertical wall. However, Mueller[29] introduced wall effects by distinguishing spheres in contact with the vertical wall, and spheres in contact with other spheres only. This method, used in this work, has been described and tested in detail in Magnico.[27]

Hydrodynamic and heat-transfer simulation method

In a second step, the velocity field is computed at the pore scale. Two main methods are currently used to compute numerically the velocity field: (a) the fluid is a continuous phase; the 3-D Navier Stokes equations (or any equations of turbulence), and the heat balance equation are solved (by finite volume technique for example); (b) the fluid is composed of particles moving and interacting on a lattice; the lattice Bolzmann automata (LBA) method consists of a statistical treatment of the distribution function represented by the particles. This method has the advantage of being robust in complex geometry,[25,26,30] although it seems that it cannot be used for heat-transfer simulations.[31]

In this work, the velocity field of an incompressible fluid is computed by means of the tridimensional Navier Stokes equations (direct numerical simulation) solved by the finite volume method on a collocated grid. Usually, the momentum equations are solved by means of staggered grids. In such grids, the velocity components are determined at the scalar control volume faces. Scalar means here the pressure or temperature, for example. Therefore, this method needs four sets of control volume for the 3-D case which increases the complexity compared to the collocation method. On the other hand, the coupling between the pressure and the velocity is solved correctly. Ferziger and Peric[32] demonstrated that by correcting the local pressure gradient, the collocation grid produces results as accurate as the staggered ones with no increase of the computing time. However, at the same time,

we need to compute the velocity at the center and at the faces of each cell. As for Ferziger and Peric, the SIMPLE algorithm is used, and is stabilized by means of the underelaxation method.

The viscous dissipation is computed by means of the central difference scheme (CDS). In the previous work[27] the ''deferred correction method'' was used in the computation of the convective contribution. This method consists in interpolating the upwind difference scheme (UDS) solution with the CDS one. In this work, the unsteady solution is computed. Therefore, in order to minimize the numerical dissipation, the second-order QUICK scheme is used. The time derivative is discretized with the following second-order polynomial

$$\frac{\partial \vec{U}^{n+1}}{\partial t} = \frac{3\vec{U}^{n+1} - 4\vec{U}^{n} + \vec{U}^{n-1}}{2\delta t} \tag{1}$$

where n means the time iteration number. The heat-transfer equation is solved in the two phases with the QUICK scheme for the convective term, and with the central difference scheme for the diffusion term. Owing to the memory available (2GB), it is necessary to use the first-order time discretization for the temperature

$$\frac{\partial T^{n+1}}{\partial t} = \frac{T^{n+1} - T^{n}}{\delta t} \tag{2}$$

For the fluid flow, the no-slip condition is prescribed at the interface solid/fluid. At the ends of the reactor, a periodic condition is specified for the velocity components with a prescribed pressure drop. The periodic boundary condition can be implemented only if the synthesized fixed bed also has a periodic geometry. With this aim, one part is first taken from the initial packing, and then it is duplicated. The two parts are placed end to end. The boundary between the two parts is located at the top of the computation domain. This method has the disadvantage, however, lowering the compacity between the two parts. This induces a perturbation in the heat transfer at the top of the computational domain.

In order to perform the comparison with several macroscopic models, the CFD simulations mimic the experiments described in the fourth part of the publication: a cold gas flow enters the packing and is heated at the wall. Therefore, an inlet temperature and a wall temperature is specified, and the oulet temperature is extrapolated. In the presence of a temperature profile in the axial direction, the periodic flow solution can be computed only if the viscosity and the density are independent of the temperature. We also assume that the thermal diffusion and the specific heat capacity are independent of temperature.

The momentum balance equations do not depend on temperature, but the energy balance equation is coupled with the momentum ones through the convective term. Therefore, at the first step, a steady flow field is computed with the first-order UDS. Then this flow field is used as the initial solution for the unsteady computation. As mentioned, above the QUICK scheme is used at this step. After n time steps, the instability is established, a stationary solution of temperature is computed with the velocity field at time t^n. Then the complete unsteady computation can start. At each time step, the unsteady velocity field is computed first, and the new solution $\vec{U}(\vec{r}, t^{n+1})$ is used to compute the unsteady solution of temperature $T(\vec{r}, t^{n+1})$.

The simulations are carried out with the same packings as in Magnico[27]: ($d_t/d_p = 5.96$ and 7.8). In order to have fixed beds with a representative volume, the bed length L is 11.5 d_p ($d_t/d_p = 5.96$) and 13d_p ($d_t/d_p = 7.8$), so that the packings are filled with 326 and 620 spheres, respectively. In order to compare the numerical approach with the heat-transfer models, the flow rate must be high enough to reach Reynolds number values higher than 100. A high Reynolds number means small time steps and high-spatial resolution. In the previous study, it was shown that the sensitivity of the velocity to the space resolution (d_p/δ) increases with the Reynolds number. The shape of the probability distribution function (pdf) of the axial velocity does not converge at a Reynolds number of 60 even with a space resolution of 40. It was also shown that the pdf is sensitive to the scheme used to approximate the convective term in the Navier Stokes equations. With the resolution of 40, the number of voxel is about 9.6×10^6 ($d_t/d_p = 5.96$), and 18×10^6 ($d_t/d_p = 7.8$) for the hydrodynamic. For the temperature inside the two phases, the voxel number is about 20×10^6 ($d_t/d_p = 5.96$), and 40×10^6 ($d_t/d_p \times 7.8$). In this study, the Reynolds number range corresponds to the unstable hydrodynamic regime. The unsteady computation requires the storage of the velocity and temperature fields at time t^{n+1}, t^n and t^{n-1}. Therefore, it is decided to use the same spatial resolution with Reynolds number values lying between 80 and 160. The value of the time step is kept constant so that the CFLmax for each velocity component is lower than 0.9 in the overall domain.

In all the simulations, the inlet gas temperature is 293 K, and the wall temperature is 373 K. The packings, through which air is flowing, are filled of ceramic spheres. The particle-to-gas conductivity ratio is 40, and the fluid Prandt number is 0.7. In all models of heat transfer, a stationary state is assumed. Therefore, the specific heat capacity of the solid phase (C_{ps}) does not appear in the heat balance equation, even in the two phase model of Dixon and Creswell.[2] The designation of the ceramic is never mentioned in experimental work. Therefore, it was decided to assume that $C_{ps} \sim C_{pf}$. This approximation has no influence on the heat transfer because, even in the unsteady hydrodynamic regime, the solid temperature remains constant.

Hydrodynamic Results

The velocity field is the key parameter for the numerical computation for the following reason. The nonlinear momentum equations control the convective transport of temperature. However, the physical and thermal properties of the fluid are independent of temperature. Hence, the linear energy balance equation does not influence the hydrodynamics. Several parameters control the accuracy of the computation: the grid size, time step, and convergence rate. Therefore, the first question is: does the hydrodynamic instability appear at the right critical Reynolds number? The hydrodynamics is sensitive to the pore space heterogeneity inside the packing filled with impermeable particles. Thus, the second question is: does the evolution of the radial profile velocity

with the Reynolds number agree with the experimental observations?

Instability threshold

Figure 1 shows the time evolution of the transversal component averaged over the whole of the packed bed ($d_t/d_p = 5.96$). The axial velocity displays no oscillations whatever the Reynolds number. The initial draft steady velocity field is far from the solution of the unsteady momentum equations. The use of this initial solution generates a perturbation which is at the origin of stable oscillations if the Reynolds number value is higher than the critical one. At a Reynolds number of 80, the solution oscillates around the final one. The amplitude decreases continuously until the steady state is reached. The same behavior is observed when the unsteady flow field at $Re_p = 120$ is used as the initial solution. This confirms that the flow is stable at $Re_p = 80$. At higher Reynolds number, the unsteady flow persists. The magnitude of the oscillation increases drastically by a factor of ten as Re_p increases from 120 to 160, i.e., an increase of 30%, although the period remains equal to about 0.4τ. In this range of Reynolds number, no erratic evolution of the velocity appears although at $Re_p = 160$, small and high magnitude of oscillations appear with a period of about 3 τ. This means that the flow is not turbulent even at the highest Reynolds number, and that a second instability mode appears as we are close to the turbulent threshold.

The critical Reynolds number value lies between 80 and 120. This was also observed by Hill et al.[33] The lattice Boltzmann approach was used in random packings made of 16 to 64 spheres. The packing was not bounded by a wall. From their data, it seems that the critical Reynolds number increases with the sphere number, but depends slightly on the solid fraction. The critical Reynolds number ranges from 80 to 100 if the sphere number is 64, with a porosity ranging from 38% to 45%.

Several experimental investigations of the hydrodynamic regimes in fixed beds was carried out[34–37] by electrochemical measurements, flow visualisation or LDA. The critical Reynolds number ranged from 90 to 150 depending on the particle shape, the packing structure and the experimental technique. More recently, Seguin et al.[38] measured the onset instability with electrochemical microprobes at the wall and in the core of the packed beds. In the case of spheres ($d_t/d_p = 7.5$ and 12), the authors found a critical Reynolds number value ranging from 110 to 120 in the core of the packing, and a critical value of about 135 at the wall. Using an NMR technique for a simple cubic array of spheres, Suekane et al.[39] observed an instability threshold at a Reynolds number value of 90. The periodicity was around 0.55τ. Unfortunately the authors do not mention what was the velocity component.

Radial distribution of the superficial axial velocity

Two research groups measured the radial profile of the axial velocity in order to validate the Brinkman-Forchheimer equation. This phenomenological equation interpolates two scales. The particle scale is modeled by the viscous dissipation term, and the Darcy scale is modeled by the Darcy/Forchheimer pressure drop correlation. If the equation is

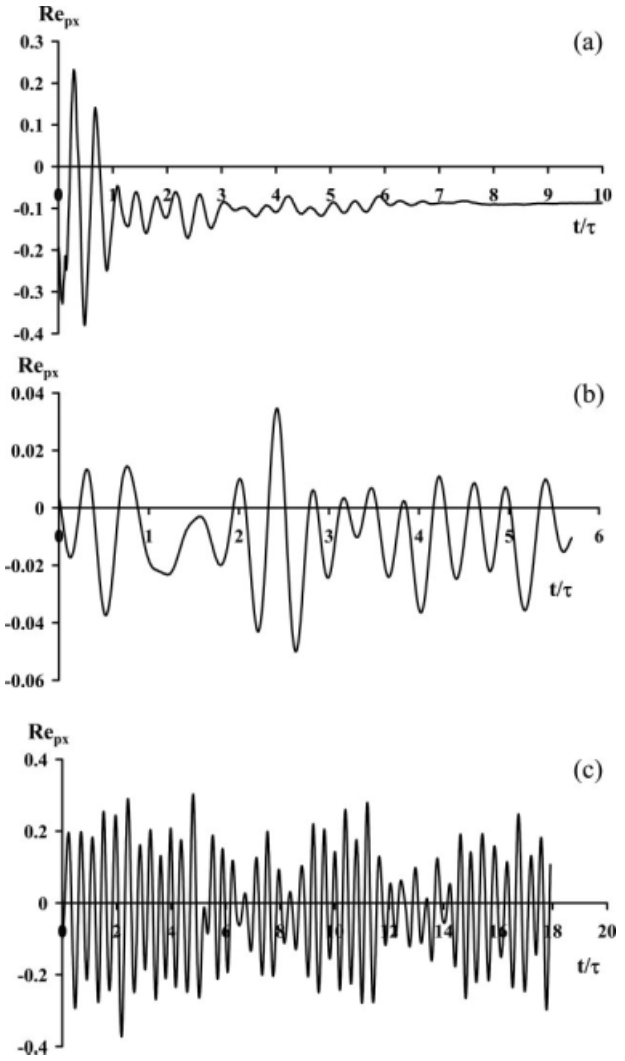

Figure 1. Time evolution of the Reynolds number (x component) averaged over the whole sphere packing defined by $d_t/d_p = 5.96$.

(a) $Re_p = 80$, (b) $Re_p = 120$, and (c) $Re_p = 160$.

extended to heterogeneous porous media by substituting the constant porosity for the local one $\varepsilon(r)$, the velocity can be computed continuously from the wall, where the viscous term is dominant ($\varepsilon \sim 1$), to the core of the packing where the Darcy/Forchheimer correlation is dominant ($\varepsilon \sim 0.4$). However, the fluid viscosity inside the viscous term has to be replaced by an effective viscosity depending on the Reynolds number, the diameter ratio and the particle shape. If the Ergun correlation is used, the extended Brinkman-Forchheimer equation is expressed as follows

$$\frac{\partial P}{\partial z} = \frac{\eta_{eff}}{r}\frac{\partial}{\partial r}\left(r\frac{\partial U_z(r)}{\partial r}\right) - AU_z(r) - BU_z^2(r)$$

$$\text{with } A = 150\frac{(1-\varepsilon(r))^2}{\varepsilon(r)^3}\frac{\eta_f}{d_p} \text{ and } B = 1.75\frac{(1-\varepsilon(r))}{\varepsilon(r)^3}\frac{\rho_f}{d_p}. \quad (3)$$

Inside fixed beds, Giese et al.[9] measured the interstitial velocity by means of laser Doppler anemometry (LDA). The

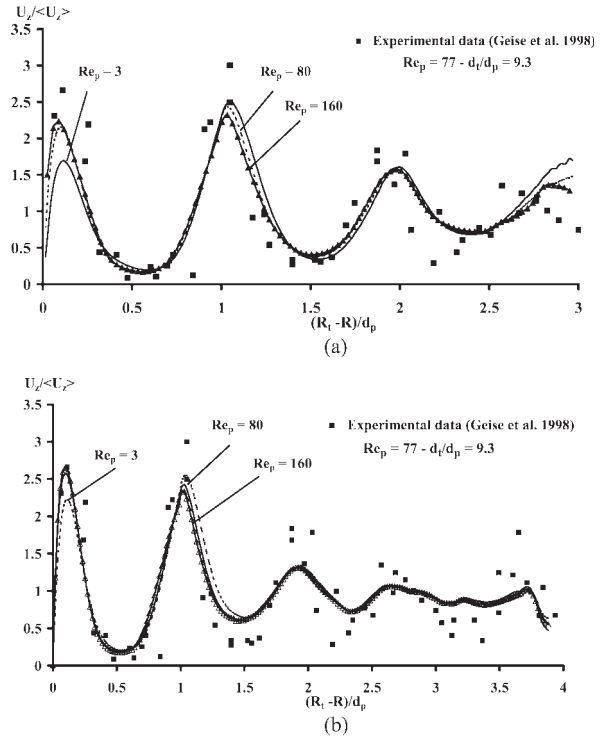

Figure 2. Radial profiles of the normalized axial velocity for three Reynolds number values: Re_p = 80, 120 and 160.

(a) $d_t/d_p = 5.96$, and (b) $d_t/d_p = 7.8$. Comparison between the CFD simulations and the experimental data of Giese et al.[9]

superficial velocity is obtained by including zero velocity inside the particles. By this method, the radial profile of porosity can also be measured whatever the particles shape. A Fourier series was used in order to match the experimental profiles of porosity.[40] Four shapes of particle were used (sphere, cylinder, deformed sphere and Raschig ring), with a diameter ratio d_t/d_p of 9.3. The Reynolds number ranged from 4 to 500. For all the particle shapes, the Ergun correlation was used. Bey and Eigenberger[10] measured, by means of hot wire anemometry, the gas velocity at the exit of a monolith positioned below the packed beds. The fluid flow was computed in the monolith and in the porous medium. As for Giese et al.[9] an analytical expression of the porosity profile, depending on the particle shape, was developed from published data. From their experiments, the two groups evaluated an effective viscosity correlation which is compared later. Another investigation was carried out by Ren et al.[41] by means of the NMR velocimetry. Spheres and pellets were used. The sphere packing had a diameter ratio lying between 1.4 and 32. The Reynolds number ranged from 6 to 225, and no viscosity correlation was suggested.

In Figure 2, the radial profiles of the normalized axial velocity computed inside the two packings are shown. The velocity at each radial position is averaged over the tangential direction and over time. The simulations carried out at four Reynolds numbers are compared with the experimental data published by Giese et al.[9] The velocity profile at a Reynolds number of 77 is chosen because, in the investigated range from 77 to 532, the radial distribution does not change significantly compared to the data scatter, and because it corresponds to the mean value of the Reynolds number range investigated in this chapter. As observed by Magnico,[27] the velocity profile in the case $d_t/d_p = 5.96$ displays a first peak, which is too small compared to the LDA data at small Reynolds number, whereas in the core region the profile is comparable. In Figure 2b ($d_t/d_p = 7.8$), the profile matches the experimental data near the wall, but in the core region the amplitude of the velocity oscillation is too small. In the Reynolds range of 3 to 80, the first peak close to the wall increases so that the two first peaks have a comparable magnitude. If $Re_p > 80$ the profile remains unchanged. In the core region, the profile is independent of the flow rate.

In order to compare the numerical results with the data of Bey[10] and Giese[9] at several Reynolds numbers, the profiles computed from the Brinkman-Forchheimer equation are used (Figure 3). Two reasons for this choice: first, this allows using comparable data because the *in situ* velocity profile of Bey and Eigenberger is deduced from experimental data outside the packings. Second, the scatter of the LDA data is large and the computed profiles from the Brinkman-Forchheimer equation match these data over all the Reynolds number range. The computed profiles of Bey and Giese will be considered as the experimental profiles. The velocity profile published by Ren et al. corresponds to $d_t/d_p = 4.8$. Therefore, the velocity profiles computed with $d_t/d_p = 5.96$ will be used in the following discussion.

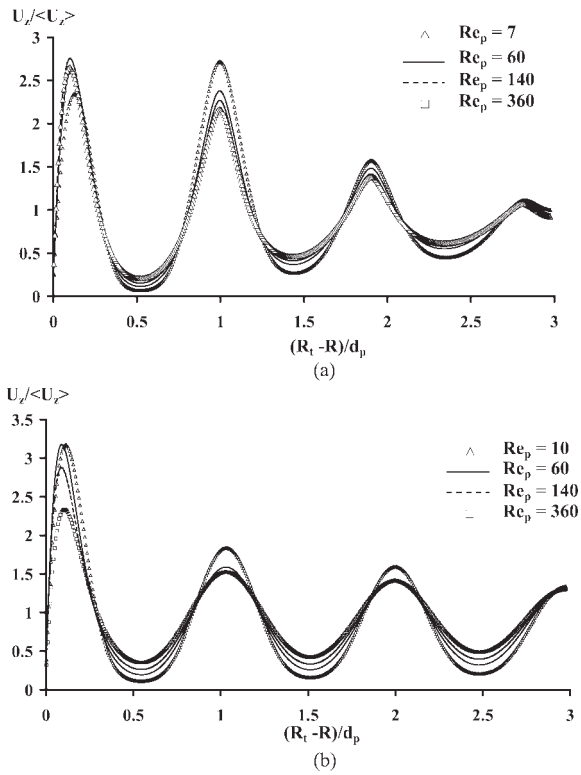

Figure 3. Radial profiles of the normalized axial superficial velocity computed with the Brinkman-Forchheimer equation.

Packing with $d_t/d_p = 5.96$. (a) Correlation of Giese et al.[9] and (b) Bey/Eigenberger correlation.[10]

The velocity profiles computed by Bey and Eigenberger from their measurements are very different from the profiles of Giese. In Figure 3a, at small Reynolds number, the second peak is higher than the first. This peak increases with the Reynolds number, and remains stable at $Re_p > 60$. The second peak decreases over the whole range of Reynolds number, although the decrease is much smaller if $Re_p > 60$. In Figure 3b, the first peak is much higher than the second peak at small Reynolds number. The magnitude of the first peak decreases if $Re_p > 60$, but the magnitude of the second peak decreases with Re_p even if $Re_p < 60$. The radial profile of the velocity depends both on effective viscosity correlation and on the porosity profile. We will first compare the porosity profiles used by the two groups (Figure 4a). The magnitude of the oscillations is higher than the one displayed by the profile of Bey. If we consider that the second peak is independent of the viscous stress term, the porosity (or permeability) profile explains the difference of magnitude of the second maximum of velocity at the same Reynolds number. These observations confirm the numerical results in Figure 2. The two groups found from their measurements two different effective viscosity correlations. If the effective viscosity remains equal to the fluid one, the first peak increases with the Reynolds number.[12] The Ergun correlation has no influence near the wall. To stabilize the first peak, a slight increase of the effective viscosity is sufficient. Thus a large reduction of this peak is induced by a noticeable increase of effective viscosity. Therefore, the correlation of Giese must predict higher values than the correlation of Bey if $Re_p < 140$, whereas for $Re_p > 140$, the correlation of Bey must predict higher values which increase when $Re_p > 60$.

The profiles published by Ren et al.[41] show that at $Re_p = 45$, the magnitude of the first peak is 3. and decreases to a value of 1.5 as Re_p increases to 140. The second and third peaks decrease from 2. to 1.4, and from 1.5 to 1, respectively, over the same Reynolds number range. The evolution of the profile with the Reynolds number can be compared with the results shown in Figure 3b. The authors mentioned that, in this range, laminar conditions are ensured throughout all the experiments. It seems that they did not take into account the unsteady flow regime. Moreover, the statistical treatment required to obtain a time-averaged velocity was not carried out.

This numerical results can be compared to others published by Zeiser et al.[24] and Freund et al,[26] Zeiser and coworkers computed the velocity field by the Lattice Boltzmann technique. Sphere packings were synthesized by a Monte Carlo method for a tube-to-sphere-diameter ratio of 5 and 6. For the packing defined by $d_t/d_p = 6$, and $L/d_p = 6$, the porosity profile is similar to the profile computed by Bey and Eigenberger.[10] At a Reynolds number of 5, and with a spatial resolution δ/d_p of 16, the LBA predicts a velocity profile close to the profile of Bey. The magnitude of the first and second peak was 3.7 and 1.5, respectively. The same group[26] used two packings for their simulations: $d_t/d_p = 4$ with $L/d_p = 20$, and $d_t/d_p = 6$ with $L/d_p = 21$. The spatial resolution d_p/δ was 30. Improving their Monte Carlo method, the porosity profile for $d_t/d_p = 6$ agrees with the profile of Benenati et al.[42] which is comparable to the profile of Mueller.[29] The magnitude of the first peak is 2.8, and the value of the second is 1.7 at $Re_p = 50$. Comparing the results published in the two articles, the same radial profiles of velocity can

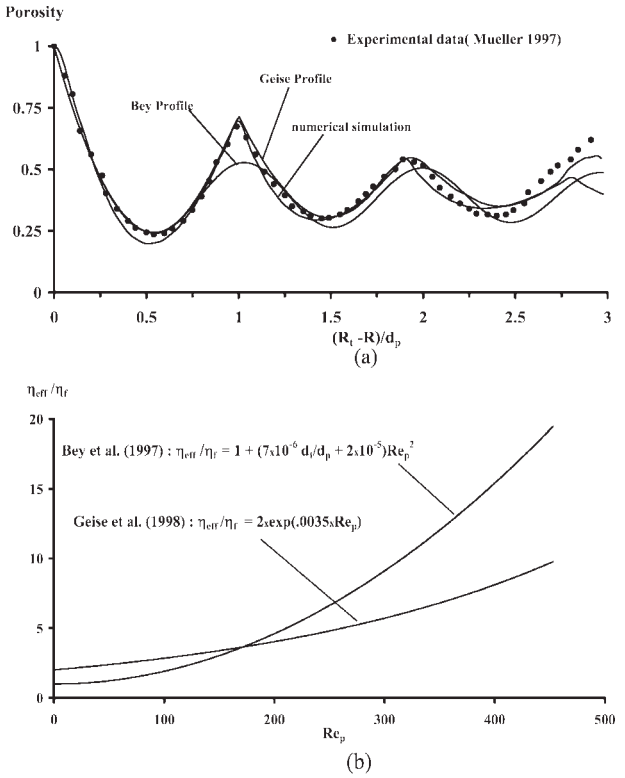

Figure 4. (a) Radial profiles of porosity, and (b) plot of the normalized effective viscosity vs. Re_p.

be obtained from two different radial profiles of porosity i.e., the velocity does not seem sensitive to the packing structure. However, in the previous publication[27], several packings with $d_p/d_t = 5.96$ were used in order to study the influence of the bed structure on the velocity profile. The simulations reveal that for the same porosity profile, the velocity profile changes drastically in the core region, the two first peaks remaining mostly identical. Thus, the porosity profile is not influenced by the packing structure contrary to the velocity profile in the core region. It is surprising that the two numerical methods (LBA and finite volume) do not compute the same velocity profile. Does this mean that the shape of the velocity profile depends on the axial boundary condition?

Heat-Transfer Models

In this section, several models are described in order to compare them with the numerical approach. They are chosen according to the coherence of their correlation set, their accuracy or the relevancy of the model.

Pseudo-homogeneous approach

To model the heat transfer in tubular fixed beds, the porous medium is considered as pseudo-homogeneous: the temperature difference between the solid and the fluid phase is not taken into account, the fixed bed is axisymmetric, heat is transferred by convection with a mean superficial velocity, and by dispersion in the radial and longitudinal directions. Generally, the three parameters are independent of the spatial coordinate. As we will see below, spatial heterogeneity

has only been taken into account recently. At high flow rate, the experimental temperature profiles display a jump at the wall. In order to take into account the heat-transfer limitation near the wall, the thin film model is used in series with the radial conductivity. At steady state, the heat balance in the absence of chemical reaction is

$$\rho_f C_{pf} U_z \frac{\partial}{\partial z} T = \lambda_r \left(\frac{\partial^2}{\partial r^2} T + \frac{1}{r} \frac{\partial}{\partial r} T \right) \tag{4}$$

with the following boundary conditions

$$\alpha_w (T_w - T) = \lambda_r \frac{\partial}{\partial r} T \quad \text{at } r = R_t \tag{4a}$$

$$T = T_O \quad at\ z = 0 \tag{4b}$$

$$\frac{\partial}{\partial r} T = 0 \quad \text{at } r = 0 \tag{4c}$$

In Eq. 1 the effective moving phase is in fact the fluid phase because it flows with the same velocity, the same density and same specific heat capacity. However, we must take into account the thermal diffusivity in the solid and the geometrical properties of the fixed bed (tube diameter, particle size, porosity). All these parameters are included in the effective thermal parameters λ_r and α_w. The effective conductivity is the contribution of two transfer mechanisms: the conduction through each phase and the hydrodynamic mixing which dominates the transfer process at high-fluid velocity. Its general expression is the sum of the two contributions

$$\lambda_r = \lambda_{0r} + \lambda_{1r} Re_p^a \tag{5}$$

Usually the wall heat-transfer coefficient α_w is expressed in the same manner even if at a small Reynolds number, its meaning is questionable. As $Re_p \rightarrow 0$ this coefficient must be considered as a lump parameter obtained by extrapolation at low Reynolds number. In fact, the sum expresses the interpolation between the two consecutive mechanisms which occur in two distinct Reynolds number ranges.

Nevertheless, even if the pseudo-homogeneous approach is easy to use, there exists a large number of correlations depending on the numerical method used for the estimation of the two coefficients. Most of the authors also observed that these coefficients depend on the fixed-bed length. The consequence is a scatter of the experimental values of α_w. Several explanations were suggested. First, the model is not able to compute the temperature profile close to the inlet with the boundary conditions (Eq. 4b and c). At the inlet, the high-temperature jump ($\Delta T = T_w - T_O$) induces a high value of the wall heat transfer. As the distance from the inlet increases, the wall heat transfer decreases and reaches an asymptotic value if the bed is long enough.[43] The location of the temperature measurement controls the estimation method and the use of the analytical solution of Eq. 4.[44,45] Second, if the pseudo-homogeneous model is used, Tsotsas et al.[4] suggested plotting the experimental data on the *Bi-Gz* diagram. The experimental data, collected by the authors, displays an independence of *Bi* toward the length ratios L/d_p and d_t/d_p over two decades in Graetz number. Third, several physical mechanisms can also influence the fluid mixing. The high-temperature close to the inlet is located at the wall. This may induce natural convection and flow instability at the wall, changing the heat transfer mechanism. Another explanation is that the velocity profile has to be developed at the inlet. One method is to use an unheated calming section, filled with the same particles as in the heated one, and located at the inlet of the packing for the velocity to develop a radial profile.[46–48]

Two main sets of correlation, computed with this heat-transfer model, are used in chemical engineering: the correlation set of Zehner/Bauer/Hennecke/Schlünder, and the correlation set of Specchia/Baldi/Sicardi, mainly based on the analysis of experimental data of many authors. Their utmost advantage lies in the determination of the two correlations the one with the other.

Zehner/Bauer/Hennecke correlations

The effective thermal conductivity and the wall heat-transfer coefficient were estimated with two different experimental setups. In the first setup, a hot gas was injected at the inlet central axis of the fixed bed through which a colder gas was flowing.[49] The temperature profiles, measured just above the inlet and at the outlet, had a Gaussian profile. The outlet temperature profile was mainly located in the core of the fixed bed so that the heat exchange with the wall and the packing heterogeneity near the wall contributed slightly in the estimation of λ_r. The particles were spheres, the thermal conductivity and the diameter ratio d_t/d_p ranged from 0.1 W/mK to 385 W/mK and from 25 to 60, respectively. Owing to the particular experimental setup, no length dependence was observed. The Peclet number ranged from 100 to 1,000. In their correlation, the authors used the expression of λ_{0r} computed by means of theoretical studies carried out by Zehner et al.[50] Complementary experiments were carried out leading to a more accurate model.[1,51]

The wall heat transfer was measured by means of a cylindrical fixed bed bound by a porous wall composed of clay particles.[52] The packed bed was immerged in a cylinder filled with water. The dry flowing gas evaporated the water at the surface of the wall. The temperatures at the wall, the inlet and the outlet were used to evaluate the heat flux at the wall. The wall and the inlet temperatures were measured by means of thermocouples. The outlet temperature was calculated with the flow rate, and with the amount of the evaporated water measured by graduated burettes. The particles were spheres, cylinders and Raschig rings and the material was glass, copper and Styropore. The Peclet number and the diameter ratio d_t/d_p ranged from 50 to 1,500, and from 4 to 50, respectively. In order to take into account the heat transfer through the packing, the authors used the pseudo-homogeneous model with their effective thermal conductivity correlation.

Martin/Nilles correlations

In order to improve the correlations available in the literature, Martin and Nilles[53] proposed to reevaluate the Nusselt

number correlation from new experimental investigations and published data. They assumed that the effective radial conductivity follows the correlation of Zehner/Bauer, but λ_{0r} depends on the tube-to-particle diameter ratio. The experiments were performed with heated air flowing through packed beds filled with spheres. The materials were glass, ceramic and steel. The diameter ratio and the Peclet number ranged from 1 to 51, and from 10 to 1,000, respectively.

Specchia/Baldi/Sicardi correlations

The λ_r and α_w correlations were calculated for spheres, cylinders and Raschig rings by means of a large number of data published in the literature, and by means of complementary experimental results.[3,54] The Reynolds number, the diameter ratio d_t/d_p, and the heat diffusion ratio λ_s/λ_g ranged from 15 to 8,000, from 3 to 80, and from 4 to 15, respectively. The selected published data were obtained from packing having a length greater than $12d_p$ so the authors assumed the depth independence of the data analysis. They used an experimental setup composed of a calming zone and a heated section. Along the two sections, the tube was made of a stainless steel material contrary to Dixon's recommendations. The thermocouples were located radially inside the packed bed at a short distance from the exit. At the outlet, the fluid is collected in a conical chamber in order to measure the mean temperature accurately. The two parameters were correlated without particle shape dependence. The motionless contributions to λ_r and α_w were analyzed with the Kunii and Smith approach.[55] By analogy with mass transfer, the convective contribution of λ_r was analyzed with the correlation of Fahien and Smith.[56] The experimental data plot of the Nusselt number vs. the Reynolds number showed that the convective contribution of α_w did not depend on the diameter ratio d_t/d_p.

Effects of radial profile of the packing heterogeneity on the heat-transfer properties

A way to improve the pseudo-homogeneous approach is to take into account the effect of the radial distribution of packing porosity on the overall heat-transfer properties. Several hydrodynamic investigations were carried out 30 or 40 years ago by laser velocimetry or by hot-wire anemometry,[57–59] but the measurements were made at the outlet of the packing. The velocity profile depends greatly on the clearance, and the radial fluctuation of the velocity was smoothed and showed only one peak close to the wall. From these observations, the packing is often divided into two regions: a core region in which the axial velocity remains constant, and a near-wall region where the axial velocity distribution is characterized by a large gradient. The heat-transfer mechanisms occur in series from the near-wall region to the core region. Several models are based on this representation.[5,6,7,52,60,61]

In order to use a more realistic model, the radial profile of velocity ($U_z(r)$) can be taken into account in the pseudo-homogeneous model. In the case of a fixed bed bound between two parallel plates separated by a distance H, Cheng and Vortmeyer[6] solved the Brinkman equation coupled with the porosity profile of Vortmeyer and Schüster.[60] They used a second-order perturbation to compute an analytical solution of the velocity. The heat-transfer equation (4) was used but with $\lambda_r(r)$, and with a prescribed wall temperature. In order to evaluate λ_r, experimental temperature data published by Schroeder et al.[62] were analyzed. In these experiments, the temperature profile in the packing was measured by a temperature difference between the two parallel plates. The particles and the fluid were glass beads and water, respectively. The size ratio H/d_p was 5.4 and 27, and the Reynolds number ranged from 100 to 2,200. The values of the three parameters on which $\lambda_r(r)$ depends were determined by matching the experimental data with the integral expression of the local temperature computed with the experimental boundary condition. However, the temperature field depends on the heat flux at the wall and the theoretical profile is antisymmetric. In fact, the experimental profiles are not antisymmetric, and in order to estimate the heat flux the authors had to extrapolate the fluid temperature at the wall, which leads to large uncertainties at low Reynolds number.

In order to improve the approach of Cheng and Vortmeyer,[6] Winterberg et al.[7] reevaluated λ_r from many experimental data available in the literature. This time the local velocity is computed with the 1-D Brinkman-Forchheimer equation in which the porosity ϵ(r) is approximated by an exponential expression. In order to predict a value of the velocity peak close to experimental observations, the effective viscosity is evaluated with the correlation of Giese.[9] The authors assumed that λ_{0r} follows the correlation provided by Zehner and Schlünder[50] as a function of the local porosity. They assumed also that λ_{1r} does not depend on the local porosity or on the local velocity, but on the radial position and on the core-to-mean-velocity ratio. The effective thermal conductivity depends on three parameters which were not evaluated at the same time. The slope parameter which determines the rate of increase of λ_r with the Peclet number was evaluated with the local injection experiments described in Zehner et al.[49] The diameter ratio and the Reynolds number ranged from 10.1 to 65, and from 100 to 2,740, respectively. The damping parameter which determines the width of the region close to the wall in which λ_r decreases, and the exponent were evaluated with wall-heated or wall-cooled experiments. The diameter ratio and the Reynolds number ranged from 5.5 to 18, and from 24 to 1,000, respectively. The slope parameter and the exponent are found to be independent of the diameter ratio and the Reynolds number. However, the damping parameter is a function of Re_p only.

The Brinkman-Forchheimer equation predicts a radial distribution of velocity with the same shape as the porosity profile except close to the wall. Therefore, a more realistic porosity profile as measured by Benenati and Brosilow[42] or Mueller,[63] must give a velocity profile oscillating over several particle diameters. Bey and Eigenberger[10] obtained such profiles by means of hot-wire anemometry. The velocity was measured at the exit of the packing. In order to avoid clearance effects, a monolith was positioned just at the outlet. Spheres, cylinders and Raschig rings were used. The diameter ratio d_t/d_p and the Reynolds number ranged from 3.3 to 11 and from 100 to 1,000, respectively.

The heat transfer properties of cylindrical packed beds[8] were studied by means of the same experimental setup as Schroeder.[62] The two parameters, α_w and λ_r, are strongly

coupled if the experimental temperature profile data is measured from cylindrical packed beds. This coupling increases the sensitivity of the parameter estimation to experimental error. The advantage of the two parallel plates heated at different temperatures is to remove the coupling. The wall heat-transfer coefficient and the heat-transfer conductivity are estimated by the temperature jump at the walls, and by the temperature gradient between the two walls, respectively. Equation 4, is, therefore, no longer used. In order to find a correlation for α_w and λ_r, measurements were performed with spheres, deformed spheres and Raschig rings made of glass and ceramics. The Reynolds number and the size ratio H/d_p ranged from 100 to 1,500, and from 3 to 9, respectively. However, the authors proposed no expression of the coefficient λ_{0r} despite the large range of the tube-to-particle diameter ratio used for their experiments. In this work, the Zehner model[49] is used to calculate this parameter.

At this stage, it is important to mention the heterogeneous model of the Cresswell/Dixon group. In order to take into account all heat transfer mechanisms in the pseudo-homogeneous model, the authors developed a two-temperature model.[2] An approximated analytical solution was computed and matched to the exact one of Eq. 1 in order to find an expression for α_w and λ_r in function of α_{ws}, α_{wf}, α_{fs}, λ_{rf}, λ_{rs}. This approach, extended to small and moderate Reynolds number,[47] may be predictable only if the expressions of the five parameters are known. With this objective, A. Dixon[64] used the correlations published by his group (Dixon and Labua[65]: α_{wf}, Melanson and Dixon[66]: α_{ws}), and by other authors (Dwivedi and Upadhyay[67]: α_{fs}, Kunii and Smith[55]: λ_{rs}), whereas λ_{rf}, λ_{zf}, λ_{zs} were adjustable parameters. Unfortunately the scatter of the experimental conductivity measurements, and also the disagreement between the α_w experimental data and the model are too great to consider the model to be quantitatively predictable with this set of correlations. Even if this approach gives a good insight into the heat-transfer mechanisms, it cannot be used in this context owing to its quantitative inaccuracy.

Heat Transfer Results

Before describing the CFD results and comparing them to macroscopic models, several remarks have to be made.

First at the solid/fluid interface, the structured mesh increases the specific surface area of the sphere and the mesh size may be larger than the heat boundary layer. The computation of the total specific surface of the spheres increases by 1.45. This factor can be explained if we consider the square computational cell. The hypothenus-to-cell-side ratio is equal to $2^{1/2}$. Therefore, at each face of the voxels in contact with the sphere surface, the heat flux is divided by this factor. Second, at the sphere surface, the mean temperature gradient around the sphere depends on Re_p and on the radial position of the sphere. In the case of spheres located far from the wall, the mean radial temperature gradient is lower than 0.5°K per cell size at a Reynolds number of 160. In the case of spheres contacting the wall the mean radial gradient is lower than 1.5°K per cell size at the same Reynolds number. Guardo et al.[20] studied the sensitivity of the heat transfer through the sphere surface toward the mesh density at the surface. In the case of a sphere suspended in an infinite fluid, the authors found that the Nusselt number is independent of the mesh density if the cell volume is 2×10^{-4} lower than the sphere one. The Reynolds number ranged from 3 to 3,000. In this work, the volume ratio is 8×10^{-6}.

Third the structured mesh flattens the contact point so that, with a spatial resolution of 40, the diameter of the contact surface is around 3δ. Thus, the CFD overestimates the conduction through the solid phase. However, it is difficult to quantify the effect of this overestimation on the temperature field in the Reynolds number range investigated. The radial conductivity increases with the Reynolds number. So at high values of Re_p, the contribution of λ_{0r} to the radial conductivity is small. Taking into account the effect of the contact surface, Bauer et al.[51] found that the contact surface fraction ρ_k^2 ranges from 1.5×10^{-4} to 3.5×10^{-4}. In the case of ceramics, the model predicts an increases of λ_{0r} by 3%. This correction is negligible compared to λ_{1r}: the model of Bauer predicts a decrease of the ratio $\lambda_{0r}/\lambda_{1r}$ from 1 to 0.5 as Re_p increases from 80 to 160. In this work, the value of ρ_k^2 ($=3^2/40^2$) is out of the range estimated by the model of Bauer. With this value, the model predicts an increaes of λ_{0r} by 28%. Argento and Bouvard[68] also studied the contribution of the contact surface on the heat conduction by means of numerical computation. The fluid conductivity is neglected in the simulations. In the case of two touching spheres, as in the model of Bauer, λ_{0r} increases by 8% if the value of the radius ratio ρ_k is 3/40. Cheng et al.[69] studied the conduction properties of a fixed bed filled with spheres in the presence of a stagnant fluid. Validated with published experimental data, the theoretical study predicts that for low-conductive materials such as ceramics, the contribution of the conduction through the contact surface is negligible (7%) compared to the contribution of the conduction through the stagnant fluid between spheres in contact. In the case of low-conductive materials, the authors showed also that the model of Bauer with $\rho_k = 0$ overpredicts the conductivity by more than 10% compared to their model, which agrees with the model of Kunii and Smith.[55] However, the distribution of the contact area is not reported. From now on, considering all these studies and the uncertainties about the contribution of all the conduction mechanisms around the sphere/sphere contact, the correlation of Bauer will be used without the contact surface effects.

In Figure 5, the CFD simulation without fluid flow is compared to the correlation of Zehner[49] with $d_t/d_p = 7.8$. The radial profiles show that the correlation overpredicts the temperature. At $Z = 2d_p$, the overestimation is around 3K. If λ_{0r} is computed with the radial profile of porosity suggested by Winterberg et al,[7] the temperature profiles agree with the CFD ones. However, the use of the local porosity underpredicts the temperature averaged over the cross-section: at $Z = 2d_p$, the underestimation is around 2 K. This comes from the presence of humps close to wall.

In the case of non-structured mesh, the fluid cells are highly skewed around contact points. In order to overcome this problem, the spheres can be shrunk,[21,22] but the heat flux through the contact point, i.e., through the gas between the shrunken spheres and the wall, has to be modeled. Under laminar conditions, the velocity field can be computed even with spheres in contact. In the case studied by the authors

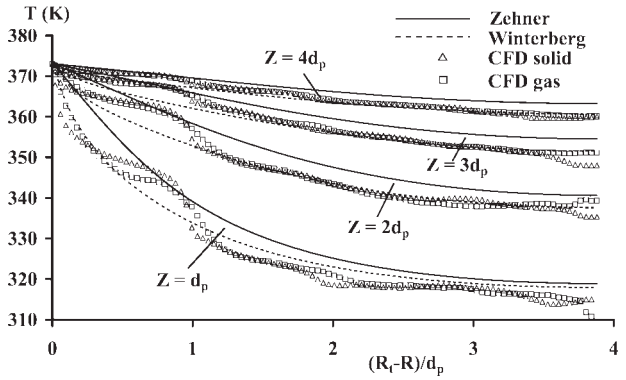

Figure 5. Radial profiles of the temperature without fluid flow; d_t/d_p = 7.8. Dots: CFD simulations (square: ceramic as solid phase, triangle: air as gas phase).

Line: Zehner correlation. Dotted line: Zehner correlation with the local porosity computed with the Winterberg correlation.

(Nylon spheres, $Re_p = 373$, $d_t/d_p = 2$, $L/d_p = 6$), a shrinkage of 1% decreases the temperature by 1.5 K at the outlet. Under turbulent conditions, CFD simulations do not converge with contacting sphere. Hence, the simulations were carried out with different shrinkage values in order to estimate the temperature increase by extrapolation to the case of contacting spheres. At $Re_p = 1922$, the temperature increase is 2 K. Another way to take into account the contact surface consists in overlapping the contacted spheres by increasing their diameter.[19] The authors used a value of 1%, but the sensitivity investigation of the heat-transfer properties toward the contact surface area has not been carried out. In the case of a structured mesh, the heat transfer around the contact points should be better taken into account if the grid adaptation is carried out in these regions.

Radial temperature profile in both solid and gas phase

In Figure 6 and 7, we compare the particle temperature and the gas temperature profiles in the two packings at a Reynolds number of 80 and 160. Contrary to the hydrodynamics, the temperature averaged over the fixed bed develops no instability, and the heat flux at the wall remains constant even if at the local scale the temperature fluctuates with the velocity, so that the radial and axial temperature profiles remain stable over time. In the two figures, the profiles are computed with the instantaneous temperature, but in order to remove statistical fluctuations especially in the fluid phase, the radial profiles are averaged over 10 cross sections.

In the two phases, the profiles show that two regions divide the fixed beds: first, a near-wall region, located at a radial distance from the wall lower than one particle

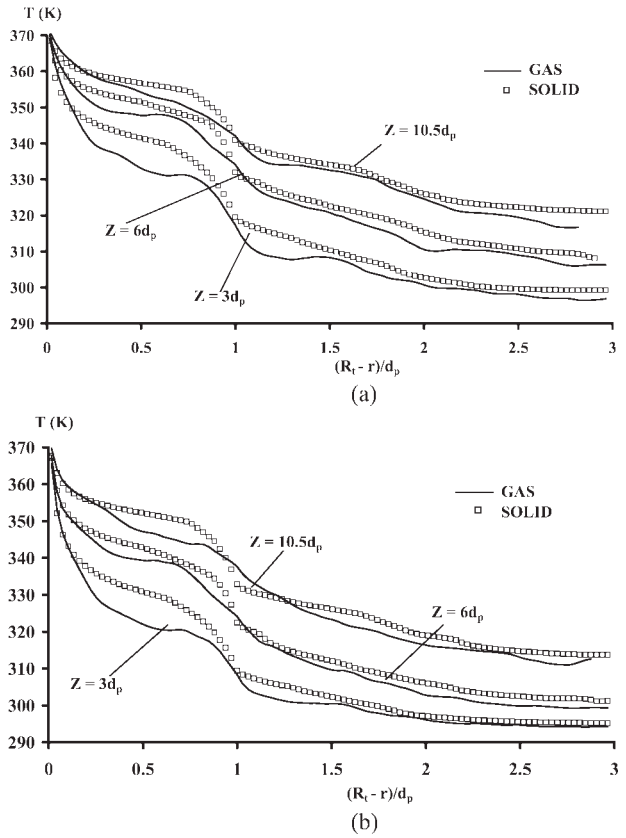

Figure 6. Radial profiles of the temperature computed by CFD simulations; d_t/d_p = 5.96; solid phase (square): ceramic; gas phase (lines): air.

(a) $Re_p = 80$, and (b) $Re_p = 160$.

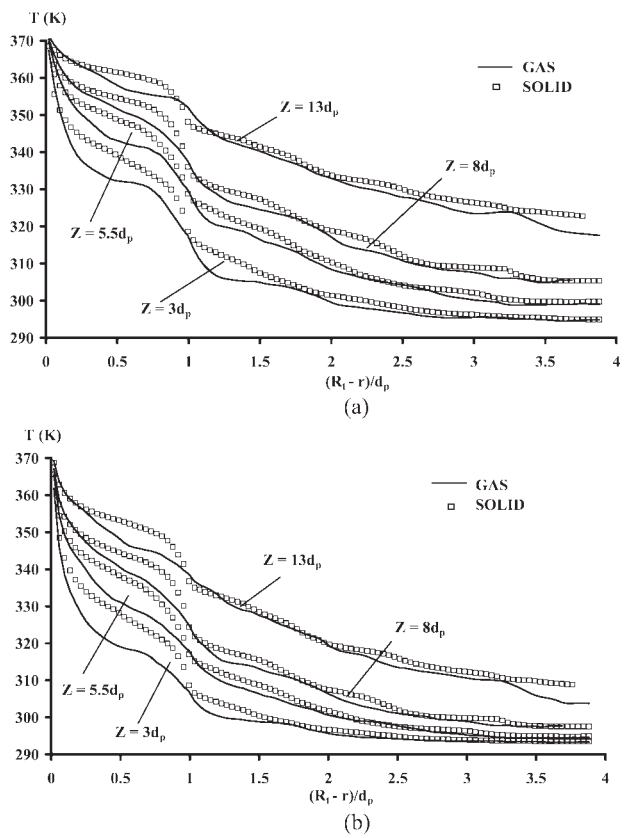

Figure 7. Radial profiles of the temperature computed by CFD simulations; d_t/d_p = 7.8; solid phase (square): ceramic; gas phase (line): air.

(a) $Re_p = 80$, and (b) $Re_p = 160$.

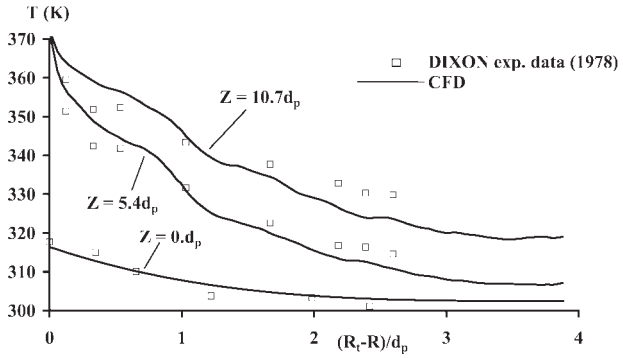

Figure 8. Comparison of the radial profile of temperature between CFD with d_t/d_p = 7.8 (line), and the experimental data of Dixon et al.[72] with d_t/d_p = 7.5, and d_p = 9.5 mm (square). Re_p = 120.

diameter, where the temperature gradient is large, and second, the core region in the remaining volume. This agrees with the experimental observations of Dewash et al[70] and Lerou et al.[71] The humps were located between d_p to $1.5d_p$ from the wall. Dixon et al[72] (see Figure 8) confirmed this observation, but the humps were located this time at $0.5d_p$ from the wall. As in Figures 6 and 7, the radial position of the humps was stable with Reynolds number. The experimental data published in 1978 must be used carefully. The authors used a brass cross to support the thermocouples. In order to avoid experimental artifacts such as conduction along the high conductive cross, A. Dixon[43] recommends using a low-conductive thermocouple cross. Therefore, the experimental data here are used only for indicative comparison and cannot be used in the following discussion. However, it seems that close to the wall, the simulations over predicts the temperature. We must also add that a radial profile of temperature is prescribed at the inlet. Its expression is $T\ (r,z = 0) = T_O + (T_w - T_O)\ (1 - r/R_T)^{\mathrm{n}}$ with $T_O = 302.5$, $T_w = 316.4$, and n = 3.1 in order to match the experimental profile at Z = 0.

If we compare the profiles at $Re_p = 80$ and at $Re_p = 160$ in Figures 6 and 7, it seems that they are independent of the hydrodynamic regime. The near-wall region can be divided into three parts, the radial location of which depends on the phase. For the solid phase, a first sub region characterized by a large temperature gradient is located against the wall. In this sub region, the two phases are at thermal equilibrium. The radial width is about $d_p/8$. It seems that the width does not change with axial position, Reynolds number or the diameter ratio d_t/d_p. A second sub region is located at a distance from the wall ranging from $d_p/8$ to $7/8d_p$ where the particle temperature is higher than the gas temperature. The temperature gradient is smaller than in the first sub region. A third sub region is located at a distance of $7/8d_p$ to d_p from the wall. The temperature gradient is high, and the temperature difference between the two phases decreases so that the two temperatures are generally close at $r = d_p$. The gas temperature fluctuates more than the particle one. In the gas phase, the three regions are not so clearly defined. The limit between the first subregion, and the second one is located between $d_p/8$ and $d_p/4$. The third one lies between $3/4d_p$ and $5/4d_p$.

The depth of the thermal equilibrium increases with the axial distance from 0 to $d_p/4$ but seems to be independent of the Reynolds number and the diameter ratio. In this sub region, the gas flows with a high-axial velocity because the first peak of the velocity profile is located at $d_p/4$. Therefore, a high-radial temperature gradient exists in the whole region. The solid temperature is located near the contact point with the wall. Around the contact point, the solid volume is so small that the tangential temperature gradient is negligible in the solid phase, and the specific surface is high enough to equilibrate the two phases.

The second sub region is located at the first minimum of the velocity profile ($U_z \sim 0.2\overline{U}z$). The solid fraction is about 75%. Therefore, the convection is no longer the dominant mechanism: the heat flux in the solid phase comes from the sphere/wall contact point to the particle center and the gas temperature is controlled by the heat flux through the solid/gas interface around the sphere/sphere contact points. So the two phases should be at thermal equilibrium. However, the convective gas transfer is small so that $T_f \sim T_s$ close to the interface particle/gas, and the temperature at the particle center must be greater than at the surface because the solid conductivity is higher than the gas one. So the two phases are not in equilibrium because at an axial position, the profile of T_s is averaged over the tangential direction and includes the temperature at the particle center.

In the region around d_p from the wall, the longitudinal gas velocity is high (see Figure 2). The gas moves mainly in the axial direction. Therefore, the heat exchange with the wall is controlled by the radial diffusion and the time to travel the sample along the radial position $r = d_p$ is much smaller than the mean residence time. Thus, the gas temperature increases slowly with the axial position. The two phases have a comparable temperature for the following reason. The solid temperature is averaged close to the solid/gas interface, where $T_f \sim T_s$ and close to the contact points where the gas is stagnant. To sum up, we have to consider that the cold gas, flowing axially with a high velocity, induces a temperature gradient in the solid phase close to the interface.

In conclusion, high-radial gradients of temperature in the gas phase are induced by the high-axial gas flow, i.e., these gradients are located at the radial position of the velocity peaks. The gas phase has a lower thermal conductivity which induces a lower temperature with a lower gradient than in the solid phase over the near-wall region. In the solid phase, the gradients are mostly located at the solid surface owing to the high-thermal conductivity. In the core region, the two phases are in thermal equilibrium and the temperature decreases slowly with increasing radial position.

Comparison with macroscopic models

In this work, the temperature profiles, computed by the microscopic approach and those by the macroscopic approach, are compared in the axial and radial direction. This avoids the effects of sample length and Reynolds number range on the parameter determination: the numerical

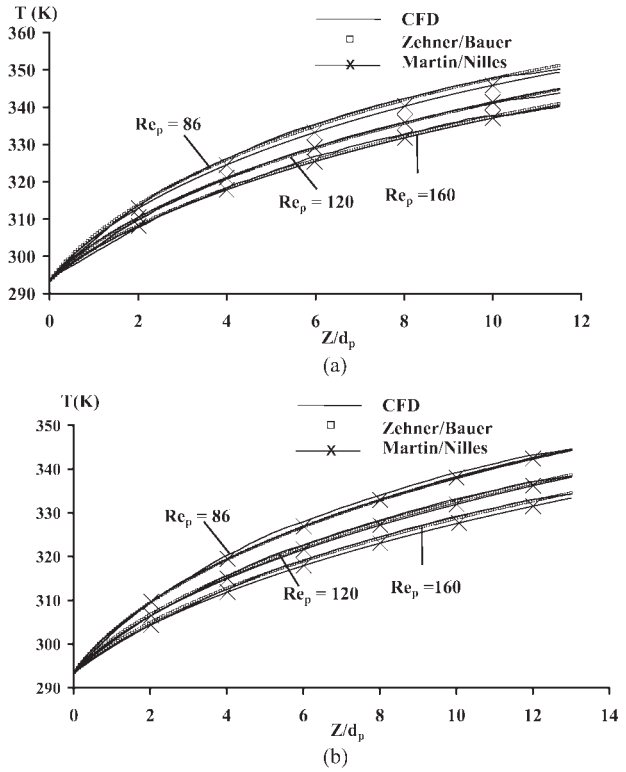

Figure 9. Axial profiles of the temperature computed with the correlations of Zehner/Bauer (square), with the correlations of Martin/Nilles (–X–), and computed by CFD simulations (line).

(a) $d_t/d_p = 5.96$, and (b) $d_t/d_p = 7.8$.

simulations show that the temperature boundary layer is not fully established. In order to compare the profiles, the temperature field of the macroscopic models is computed with the differential equation (4) solved by means of the finite volume technique according to the assumptions of each model. The porosity is assumed to be 40%. The microscopic approach separates the two phases, and the global temperature field is a combination of the temperature of each phase, i.e., this approach can be compared to the two-phase model of Dixon and Cresswell.[2] In the single-phase macroscopic models, the effective medium resembles the fluid phase, because it flows with the superficial fluid velocity. The macroscopic and the microscopic approaches can be compared if the two phases are in thermal equilibrium, and if the particle size is much smaller than the temperature gradient. We will see that it is not the case in all the samples. Despite these observations, the fluid temperature of the microscopic model will be used in the discussion.

Heat-transfer properties of fixed beds depend on several parameters. In order to check the robustness of the microscopic model, the comparison with macroscopic ones is carried out with different values of the two following parameters: d_t/d_p and Re_p. In the three macroscopic approaches of Bey,[8] Cheng[9] and Winterberg,[7] the longitudinal profile is computed by averaging the heat flux over the cross-section in the gas phase

$$\overline{T}(z) = \frac{\int_0^{Rt} U_z(r)T(r,z)rdr}{\frac{1}{2}\overline{U}_z R_t^2} \tag{6}$$

Owing to the cylindrical symmetry assumption of the pseudo-homogeneous models, the velocity is constant and equal to the mean value over a circumference. Therefore, the temperature is directly used in the radial profile computation. As in the previous section, the radial profile of the gas temperature computed by CFD is an average over 10 cross-sections.

Let us compare the CFD simulations to the pseudo-homogeneous models of Zehner/Bauer, Martin/Nilles and Specchia/Baldi, in which no radial heterogeneity is assumed. In Figure 9 the axial profiles computed with the model of Zehner/Bauer and with the CFD simulations are shown. The profiles inside the two packings agree over all the Reynolds number range. In the worst case, i.e., where $Re_p = 80$ and $d_t/d_p = 7.8$, the temperature difference is about 2 K only. Therefore, the heat balance over the porous medium is well predicted by the Zehner/Bauer model. The agreement throughout the packings also means that the length effect is

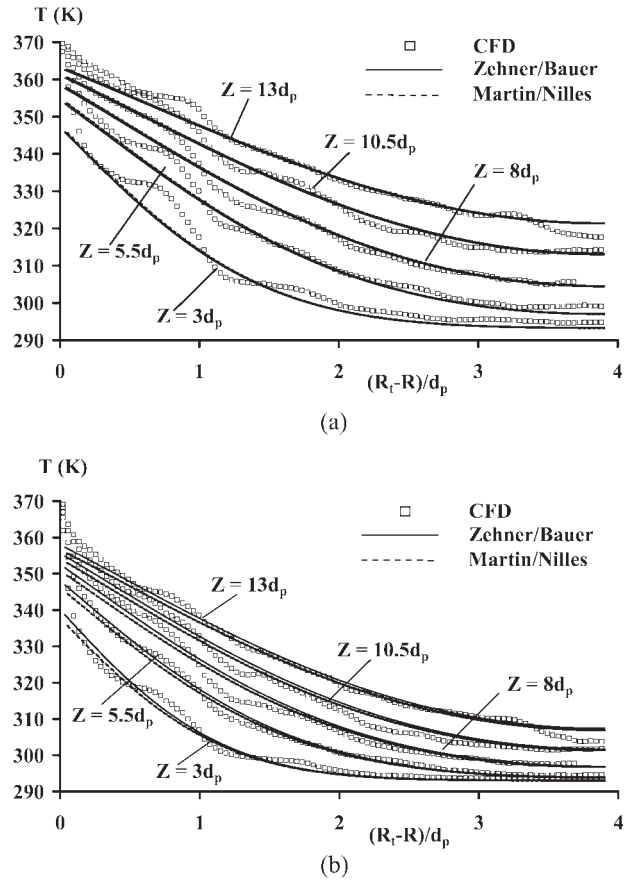

Figure 10. Radial profiles of the temperature computed with the correlations of Zehner/Bauer (line), with the correlation of Martin/Nilles (dotted line), and computed by CFD simulation (square); $Re_p = 160$.

(a) d_t/d_p =5.96, and (b) $d_t/d_p = 7.8$.

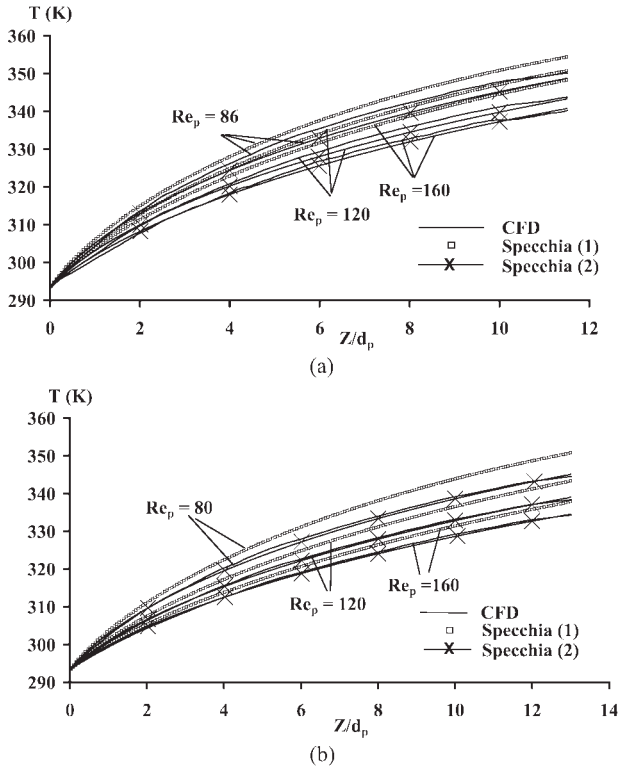

Figure 11. Axial profiles of the temperature computed with the correlations of Specchia (square) with the correlations of (Specchia + Kunii and Smith[55]) (—X—), and computed by CFD simulation (line).

(a) $d_t/d_p = 5.96$, and (b) $d_t/d_p = 7.8$.

not noticeable. In order to compare further, the radial profiles inside the fixed bed $d_t/d_p = 7.8$ are shown in Figure 10. As in Figure 7, the same thermal regions can be observed. In the core region, a thermal equilibrium is established, and the two approaches predict the same temperature. The region is localized at a radial distance from the wall greater than $1.25d_p$. In the near wall region ($R_t - r < d_p$), the sphere packing is ordered along the wall. The porosity at $R_t - r = d_p/2$ is around 25% (see Figure 4b). Therefore, the packing structure is close to the cubic face centered array. The radial heat transfer in the gas phase is small, and the gas temperature hump at R_t - $r = d_p/2$ is induced by the contribution of the heat transfer through the particle/gas interface. However, this heat flux is not sufficient to avoid the thermal disequilibrium between the two phases. At $Re_p = 80$ (Figure 10a), the humps are highly visible all along the bed length. Therefore, the pseudo-homogeneous model of Zehner/Bauer cannot predict the shape of the radial profile in the near-wall region. Against the wall, the numerical results display no thermal boundary layer, even at the outlet, owing to the small value of the Reynolds number. The pseudo-homogeneous model predicts a wall temperature jump of 10 K at the outlet, and, consequently, the model underestimates the temperature in the entire near wall region. This might explain why the axial profile of the Zehner/Bauer temperature is a little smaller. At high Reynolds number (Figure 10b) the humps are not as clear. The heat boundary layer seems to appear close to the outlet with a temperature jump of 10 K. At this axial position, the model of Zehner/Bauer predicts a jump of 15 K. Therefore, the discrepancy between the two approaches decreases as the Reynolds number increases.

The CFD results also match the model of Martin/Nilles (Figures 9 and 10). However, in Figure 9b, it seems that, in the case $d_t/d_p = 7.8$ and at high Reynolds number, the two approaches are less in agreement. Figure 10b shows that at high Reynolds number, the difference of temperature between the two macroscopic models is located close to the wall owing to the correlation of the Nusselt number used in the two models. If $d_t/d_p = 5.96$, the two macroscopic models show a small disagreement at small Reynolds number (see Figure 9a). However, the investigated range of diameter ratio and Reynolds number does not allow the two macroscopic models to be distinguished.

The model of Specchia/Baldi (Specchia 1) is compared to the CFD simulations in Figures 11 and 12. In Figure 11, the axial profiles along the two packings show a noticeable temperature difference between the two computations. The macroscopic model overestimates the radial heat transfer. The discrepancy increases with the axial position, but it decreases as the Reynolds number increases if $d_t/d_p = 7.8$. In Figure

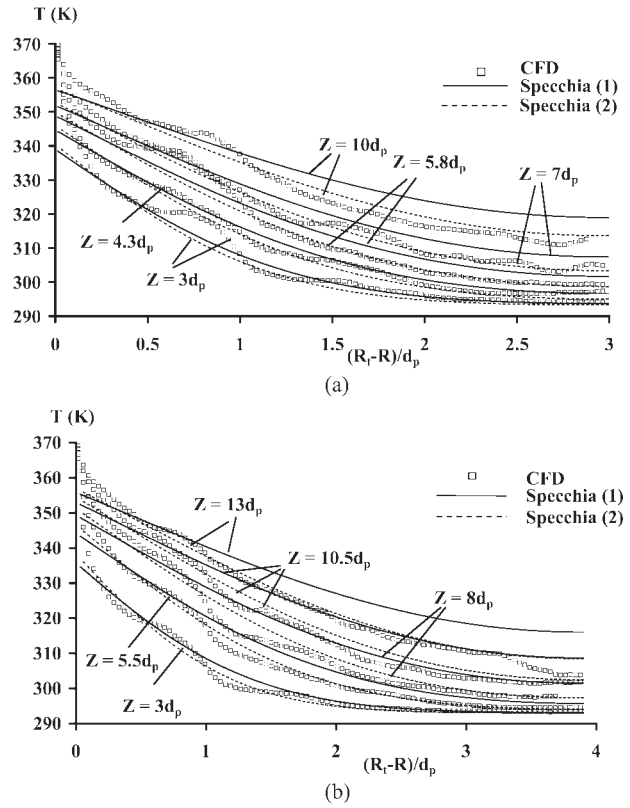

Figure 12. Radial profiles of the temperature computed with the correlations of Specchia (line), with the correlations of (Specchia + Kunii & Smith[55]) (dotted line), and computed by CFD simulation (square); $Re_p = 160$.

(a) $d_t/d_p = 5.96$, and (b) $d_t/d_p = 7.8$.

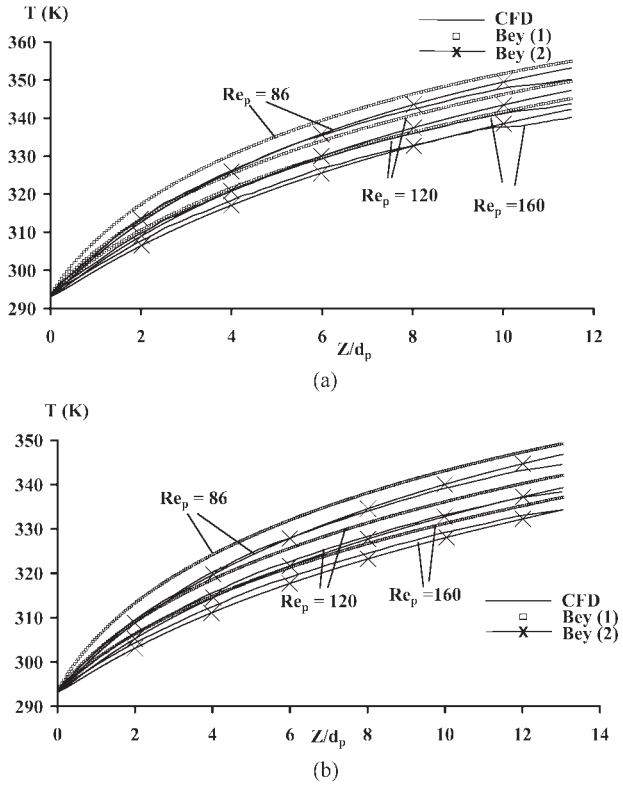

Figure 13. Axial profiles of the temperature.

Square: correlations of Bey, temperature averaged with the radial profile of velocity: —X— correlations of Bey, temperature averaged with a constant velocity. Line: CFD simulation. (a) $d_t/d_p = 5.96$, and (b) $d_t/d_p = 7.8$.

12, the radial profiles inside the two packings at $Re_p = 160$ are shown, i.e., where the discrepancy is smaller. In the core region, the model of Specchia/Baldi overpredicts temperatures. Let us compare the radial profiles in Figure 12b to the profiles computed with the model of Zehner/Bauer in the same fixed bed (Figure 10b). At the wall and close to the inlet, the temperature predicted by the former model is smaller, but this discrepancy decreases as the axial distance from the inlet increases. As observed above, the temperature computed by the correlations of Specchia/Baldi is too high in the core region. This means that these correlations overestimate the radial heat-transfer diffusivity. The discrepancy is all the greater since the Reynolds number is small. Specchia and Baldi computed the parameter λ_{0r} with the model of Kunii and Smith,[55] but they used experimental data to correlate the parameter Φ with the porosity. In Figures 11 and 12, the Specchia/Baldi model is shown but with the full model of Kunii and Smith (Specchia 2). The profiles show that if the model of Specchia/Baldi is used with the exact expression of λ_{0r} computed by Kunii and Smith, the macroscopic model agrees with the CFD simulations over the whole Reynolds range and over the length of the two packings, except for $d_t/d_p = 5.96$ at $Re_p = 80$.

Let us now compare the models which take into account the radial heterogeneity. The model of Bey/Eigenberger and the CFD simulations disagree. In Figure 13, the former model (Bey 1) predicts a higher-temperature profile whatever the diameter ratio and over all the Reynolds number range. However, for the high diameter ratio, it seems that the disagreement between the two models decreases as the Reynolds number increases. If we compare the radial profiles (Figure 14) for $d_t/d_p = 7.8$, we observe that at small Reynolds number the macroscopic model predicts a higher-temperature in the core region. Comparing this model with the model of Zehner/Bauer (Figure 10a), the model of Bey/Eigenberger also predicts higher-temperature at all radial positions. The discrepancy increases with the axial position, whereas at high Reynolds number, the two macroscopic models (Figures 10b and 14b) predict comparable temperature profiles even close to the wall and agree with the CFD computations. In fact, the model of Bey/Eigenberger predicts a temperature slightly lower as we will see later. The discrepancy between Figures 13b and 14b comes from the comparison of different quantities. The axial and the radial profiles are computed by means of the heat flux (6) and the temperature, respectively. In the model of Bey/Eigenberger, the radial velocity profile is taken into account. Therefore, contrary to the three first macroscopic models, the average heat flux is not equal to the average temperature. In Figure 13, the axial profiles (Bey 2) are computed with the temperature only. The axial temperature is smaller than the temperature computed with (6), and there is no longer any

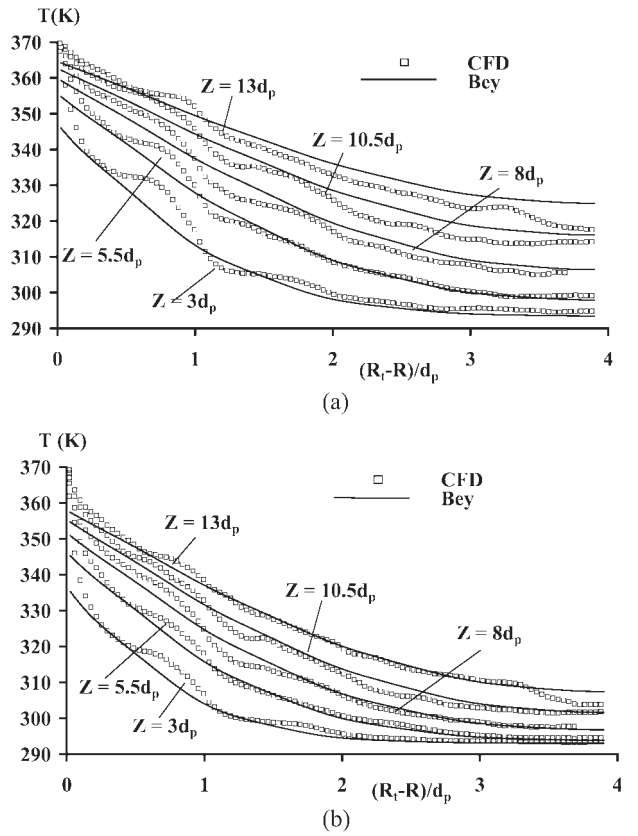

Figure 14. Radial profiles of the temperature computed with the correlations of Bey/Eigenberger (line), and computed by CFD simulations (square); $d_t/d_p = 7.8$.

(a) $Re_p = 80$, and (b) $Re_p = 160$.

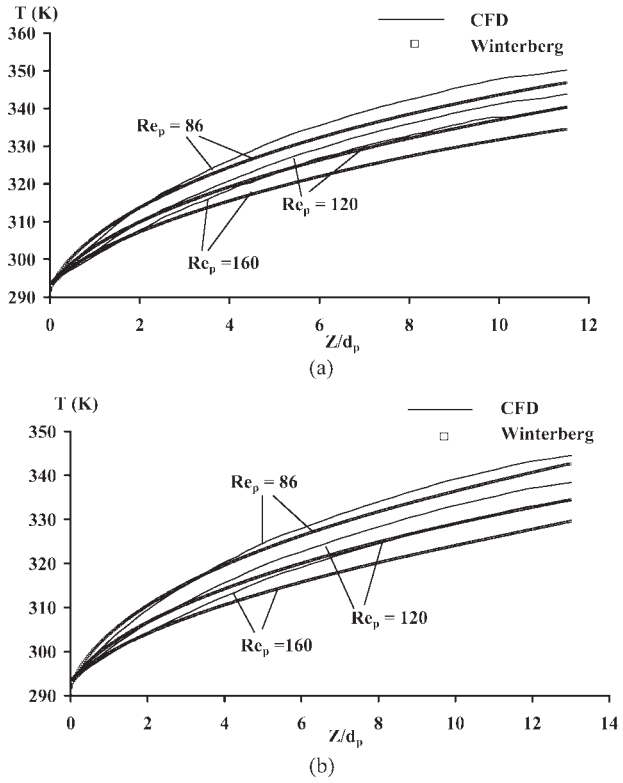

Figure 15. Axial profiles of the temperature computed with the correlations of Winterberg (square), and computed by CFD simulation (line).

(a) $d_t/d_p = 5.96$, and (b) $d_t/d_p = 7.8$.

discrepancy between the macroscopic and the microscopic models. If the axial temperature is computed with the heat flux, the integral is sensitive to the temperature located at the velocity peaks. In the region $R_t - r < 0.75d_p$, the normalized axial velocity value is higher than two, and the temperature is higher than in the core region. The temperature average is weighted by the axial velocity. Therefore, the contribution of the velocity profile in the integral (6) increases the axial temperature. In other words, if we take into account the heat balance, we have to use the average heat flux. The axial profiles show that the model of Bey/Eigenberger overestimates the radial heat flux. If we compare the axial profiles, the average temperature computed with a constant velocity could be used but it is questionable.

The model of Winterberg takes into account both the radial profile of the velocity and the radial thermal conductivity. Contrary to the other macroscopic models, the gas temperature is set equal to the wall temperature at $r = R_t$. The radial velocity profile is characterized by one peak located at $0.12d_p$ from the wall. Its magnitude is about 2.5 times the mean velocity. In the core of the fixed bed, the magnitude is 0.7 times the mean velocity. The local velocity equals the mean velocity at $0.45d_p$. These characteristic values remain constant in the range of Re_p and the diameter ratio investigated. Concerning the effective conductivity, the width of the near-wall region decreases from $1.6d_p$ to $0.83d_p$ as Re_p increases from 86 to 160. Therefore, the near-wall region of the thermal conductivity does not coincide with the velocity one. In the core region, where λ_r is constant, the correlations of Winterberg and of Bauer predict a comparable value of the radial effective conductivity. However, in the near-wall-region, the correlation of Winterberg predicts a decrease of λ_r to a value close to λ_f as the distance from the wall decreases to zero. The correlation of Winterberg, therefore, predicts a smaller value of λ_r than the correlation of Bauer whatever the radial position. Figure 15 shows that the model of Winterberg predicts a much lower temperature than the CFD computation. For the two diameter ratios, the discrepancy increases with the Reynolds number. In Figure 16, the radial profiles show that the macroscopic model predicts a decrease of the temperature far higher close to the wall owing to the small radial conductivity. At high Reynolds number (Figure 16b), a boundary layer can be seen whose width is around $0.4d_p$, which is higher than the width predicted by CFD. At this radial position, the temperature difference between the two approaches is higher than 10 K. In the core region, the discrepancy decreases as the radial distance from the wall increases.

However, at this step of the comparison, it must be noticed that in the publications[7] and,[76] the Winterberg model and the Martin/Nilles one (or model) agree with experimental data. However, the Martin/Nilles model seems to

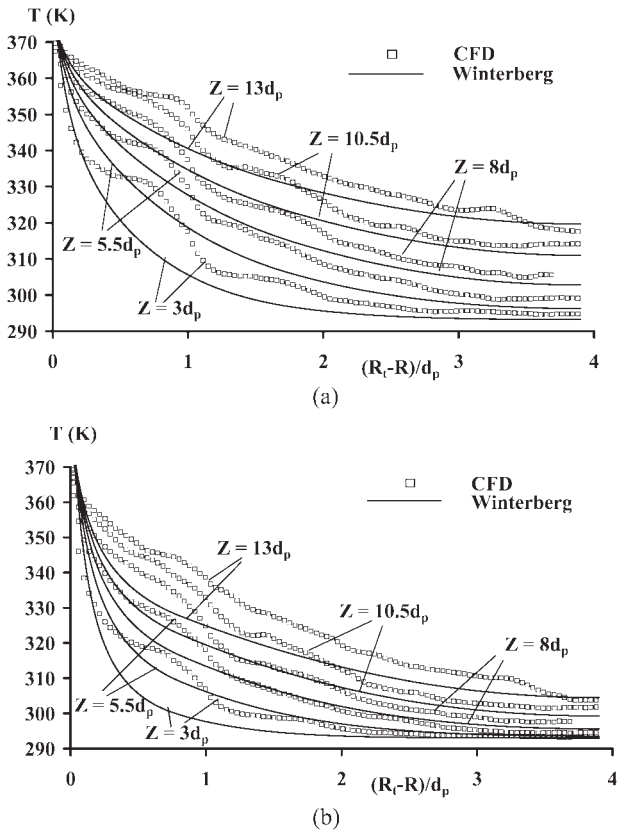

Figure 16. Radial profiles of the temperature computed with the correlations of Winterberg (line), and computed by CFD simulations (square) $d_t/d_p = 7.8$.

(a) $Re_p = 80$, and (b) $Re_p = 160$.

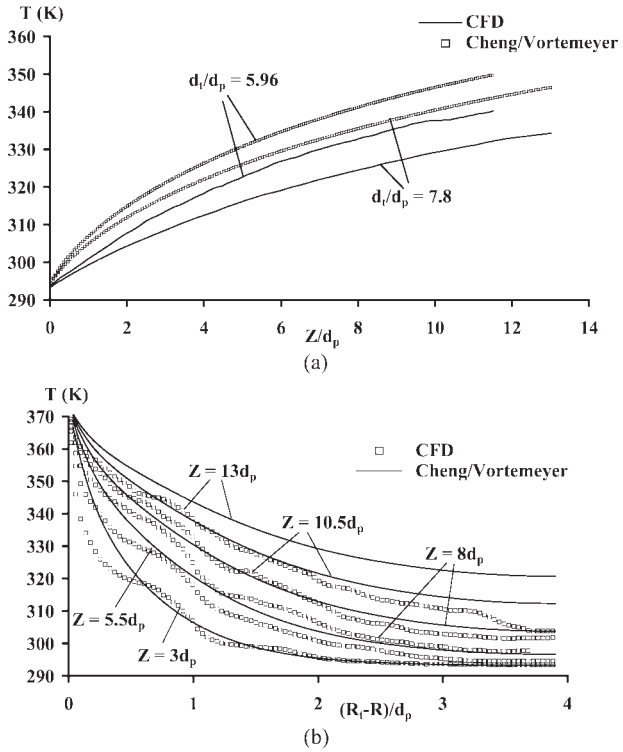

Figure 17. Temperature profiles computed with the correlations of Cheng/Vortmeyer, and computed by CFD simulations; Re_p = 160.

(a) axial profiles, d_t/d_p = 7.8 and 5.96, and (b) radial profiles, d_t/d_p = 7.8.

underpredict the local temperature. These publications show also that Winterberg model gives more realistic profiles close to the wall. In this work, the CFD agrees the Martin/Nilles model (Figure 10), and experimental data (Figure 8). However, unfortunately, for reasons that have not been elucidated until now, the Winterberg model disagrees with the CFD results, and also with the Martin/Nilles model. Therefore, no conclusion can be drawn from the comparison between the microscopic approach and the Winterberg model. In the appendix, all the correlations used in this model are introduced, and the radial profiles of the velocity and of the effective radial conductivity used in the simulations are shown.

The model of Cheng localizes the velocity peak at $d_p/3$ from the wall. Its magnitude is about twice the mean velocity. In the core of the fixed bed, the magnitude is one half the mean velocity. The near-wall region lies over $2.5d_p$ from the wall, i.e., over most of the cross-section of the two packings. In this region, the heat conductivity increases from the stagnant conductivity to about twice the value predicted by the model of Zehner/Bauer for the two packings. The two models predict the same value at about $r = d_p$ from the wall. In Figure 17, the model is compared to the CFD simulations at $Re_p = 160$. In Figure 17a, the axial profiles along the two packings display a high discrepancy compared to the CFD simulations. The over prediction increases with the axial position. This discrepancy is confirmed by the radial profiles in Figure 17b ($d_t/d_p = 7.8$). In fact, the macroscopic model overestimates the radial heat-transfer conductivity over most of the cross-section. Therefore, its overestimated value in the core region cannot be compensated by the small value of the radial heat conductivity close to the wall.

Guardo et al.[19] studied the heat transfer properties of a fixed bed, filled by 44 spheres ($d_t/d_p = 3.92$), which seemed to be nonconductive. Several turbulence models, available in the commercial code Fluent, were used in order to compare the Nusselt number and the effective heat-transfer coefficient to correlations in the Reynolds number range lying from 100 to 900. The authors found that the numerical results agree with the α_w correlation of Olbrich and Potter[74] and the λ_r correlation of Yagi and Wakao.[46] However, the hypothesis of nonconductive spheres makes their numerical results unrealistic. Moreover, the authors used self-consistent correlations and models: α_w and λ_r correlations were determined simultaneously by experimental investigations[46,75] or by theoretical ones.[2] The agreement may be stated only if the numerical results match the two correlations simultaneously. Therefore, their analysis seems to be incoherent. Freiwald and Paterson (1992) also tempted to carry out model discrimination by means of their experimental data and the Dixon's ones. The Reynolds number ranged from 50 to 1,300. Spheres, cylinders and Raschig rings were employed. The authors found that the model of Zehner/Bauer for λ_r, and the model of Hennecke for α_w agreed best with the experimental results.

Conclusion

Over many publications, it has been demonstrated that the macroscopic approach cannot accurately describe the heat-transfer mechanism in packed beds. Several research groups have attempted to improve the pseudo-homogeneous model by introducing radial heterogeneity or by taking into account explicitly the thermal property of the two phases. However, most of these models do not give quantitative predictions. In this work, another approach has been used. It consisted in computing the velocity and temperature field at the pore level by means of direct numerical simulation and resolution of the heat balance equation. It was shown that at Reynolds number ranging from 80 to 160, the numerical results agree with the experimental observations concerning the radial profile of the axial velocity and the prediction of the hydrodynamic instability threshold. The computation of the temperature field has shown that along the wall the two phases are not at thermal equilibrium over a layer the depth of which is one diameter. The radial temperature profiles also revealed the existence of humps over this layer. Against the wall a thermal boundary layer appears at Reynolds number values higher than 120. Its depth is about $d_p/8$.

Several macroscopic models were used in order to verify the accuracy of the simulation. A detailed comparison of radial and axial profiles has shown that the model of Zehner/Bauer/Hennecke and of Martin/Nilles agree best with the numerical simulations. However, close to the wall, this model does not agree with the CFD simulations owing to the thermal disequilibrium between the two phases, and also the thermal boundary layer weakly developed in the Reynolds number range investigated. The model of Specchia/Baldi overestimates the radial stagnant heat transfer conductivity. The model can be improved if the complete model of Yagi and Kunii is applied. Unfortunately, the interesting model of

Bey and Eigenberger, which takes into account a realistic radial profile of velocity, does not agree with the simulations. Even if the radial profiles match the CFD simulations, it overestimates the radial heat transfer. Unfortunately, CFD simulations disagree with the models with a radial profile of effective conductivity.

The comparison of several macroscopic models and experimental data shows that the direct numerical simulation in 3-D artificial packing with no hydrodynamic assumptions, allows realistic results to be obtained and the microscopic mechanism of heat and mass transfer to be accessed in the case of a small temperature gradient. However, the solid surface (wall and spheres), and the contact points (sphere/sphere and sphere/wall), cannot be described accurately by the use of structured mesh. An unstructured mesh is more suitable for complex topology, but its use needs more memory requirement. This work could be improved by increasing the resolution around the contact points using a grid adaptation. Another improvement would consist in the use of the immersed boundary method in order to better define the solid surface.

Notation

C_p = gas specific heat capacity under constant pressure, J $kg^{-1}K^{-1}$
d = diameter, m
L = fixed-bed length, m
P = pressure $Kgm^{-1}s^{-2}$
R = radius, m
T = temperature, K
T_Q = temperature at the inlet, K
$\vec{U}$ = superficial velocity ms^{-1}
r = radial coordinate, m
t = time, s
z = axial coordinate, m
— = cross-section average
$< >$ = average over the fixed bed

Greek letters

α = heat-transfer coefficient, $Wm^{-2}K^{-1}$
δ = grid size, m
δt = time step, s
ε = porosity
η = dynamic viscosity, Kg $m^{-1}s^{-1}$
η_{eff} = effective fluid viscosity, Kg $m^{-1}s^{-1}$
λ = thermal conductivity $Wm^{-1}K^{-1}$
ρ = density, Kg m^{-3}
τ = mean time for a fluid to travel a sphere diameter $\frac{d_p \varepsilon}{<U_z>}$, s

Subscripts

c = core
f = fluid
p = particle
r = radial component
z = axial component
x,y = transversal component
s = solid
t = tube
w = wall
0 = conductive contribution
1 = convective contribution

Dimensionless numbers

$Bi = \alpha_w R_t/\lambda_r$ = Biot number
$Gz = Pe_r\, d_t^2/Ld_p$ = Graetz number
$Pr = C_{pf}\, \eta_f/\lambda_f$ = Prandt number
$Re_p = \rho_f <U_z> d_p/\eta_f$ = Reynolds number

Literature Cited

1. Bauer R, Schlünder EU. Effective radial thermal conductivity of packings in gas flow. Part I. Convective transport coefficient. *Int Chem Eng*. 1978;18;181–189.
2. Dixon AG, Cresswell DL. Theoretical prediction of effective heat transfer parameters in packed beds. *AIChE J*. 1979;25;663–676.
3. Specchia V, Baldi G, Sicardi S. Heat transfer in packed bed reactors with one phase flow. *Chem Eng Comm*. 1980;4;361–380.
4. Tsotsas E, Schlünder EU. Heat transfer in packed beds with fluid flow: remarks on the meaning and the calculation of a heat transfer coefficient at the wall. *Chem Eng Sci*. 1990;45;819–837.
5. Kunii D, Suzuki M, Ono N. Heat transfer from wall surface to packed beds at high Reynolds number *J Chem Eng Jpn*. 1968;1; 21–26.
6. Cheng P, and Vortmeyer D. Tranverse thermal dispersion and wall channelling in a packed bed with forced convective flow. *Chem Eng Sci*. 1988;43;2523–2532.
7. Winterberg M, Tsotsas E, Krischke A, Vortmeyer D. A simple and coherent set of coefficients for modelling of heat and mass transport with and without chemical reaction in tubes filled with spheres. *Chem Eng Sci*. 2000;55;967–979.
8. Bey O, Eigenberger G. Gas flow and heat transfer through catalyst filled tubes. *Int J Therm Sci*. 2001;40;152–164.
9. Giese M, Rottschäffer K, Vortmeyer D. Measured and modeled superficial flow profiles in packed beds with liquid flow. *AIChE J*. 1998;44;484–490.
10. Bey O, Eigenberger G. fluid flow through catalyst filled tubes. *Chem Eng Sci*. 1997;52;1365–1376.
11. Givler RC, Altobelli SA. A determination of the effective viscosity for the Brinkman-Forchheimer flow model. *J Fluid Mech*. 1994; 258;355–370.
12. Papageorgiou JN, Froment GF. Simulation models accounting for radial voidage profiles in fixed bed reactors. *Chem Eng Sci*. 1995; 59;3034–3056.
13. Vortmeyer D, Haidegger E. Discrimination of three approaches to evaluate heat fluxes for wall-cooled fixed bed chemical reacteors. *Chem Eng Sci*. 1991;46;2651–2660.
14. Coelho D, Thovert JF, Adler PM. Geometrical and transport properties of random packings of spheres and aspherical particles. *Phys Rev E*. 1997;55;1959–1977.
15. Martys N, Torquato S, Bentz DP. Universal scaling of fluid permeability for sphere packings. *Phys Rev E*. 1994;50;403–408.
16. Salles J, Thovert JF, Delannay R, Prevors L, Auriault JL, Adler PM. Taylors dispersion in porous media. Determination of the dispersion tensor. *Phys Fluids*. 1993;A5;2348–2376.
17. Calis HPA, Nijenhuis J, Paikert BC, Dautzenberg FM, van den Bleek CM. CFD modelling and experimental validition of pressure drop and flow profile in a novel structured catalytic reactor packing. *Chem Eng Sci*. 2001;56;1713–1720.
18. Gunjal PR, Ranade VV, Chaudhari RV. Computational study of single phase flow in packed beds of spheres. *AIChE J*. 2005;51; 365–377.
19. Guardo A, Coussirat M, Larrayoz MA, Recassens F, Egusquiza E. Influence of the turbulene model in CFD modelling of wall-to-fluid heat transfer in packed beds. *Chem Eng Sci*. 2005;60;1733–1742.
20. Guardo A, Coussirat M, Recassens F, Larrayoz MA, Escaler X. CFD study on particle-to-fluid heat transfer in fixed bed reactors: Convective heat transfer at low and high pressure. *Chem Eng Sci*. 2006;61;4341–4353.
21. Nijemeisland M, Dixon AG. CFD study of fluid flow and wall heat transfer in a fixed bed of spheres. *AIChE J*. 2004;50;906–921.
22. Nijemeisland M, Dixon AG. Comparison of CFD simulations to experiment for convective heat transfer in a gas-solid fixed bed. *Chem Eng J*. 2001;82;231–246.
23. Mantz B, Gladden LF, Warren PB. Flow and dispersion in porous media: lattice Boltzmann and NMR studies. *AIChE J*. 1999;45; 1845–1854.
24. Zeiser Th, Lammers P, Klemm E, Li YW, Bernsdorf J, G. Brenner G. CFD-calculation of flow, dispersion and reaction in a catalyst filled tube by the lattice Boltzmann method. *Chem Eng Sci*. 2001;56;1697–1704.
25. Yuen EHL, Sederman AJ, Sani F, Alexander P, Gladden LF. Correlation between local conversion and hydrodynamics in a 3-D fixed-

bed esterification process: an MRI and lattice-Boltzmann study. *Chem Eng Sci*. 2003;58;613–619.
26. Freund H, Zeiser T, Florian H, Klemm E, Brenner G, Durst F, Emig G. Numerical simulations of single phase reacting flows in randomly packed fixed-bed reactors and experimental validation. *Chem Eng Sci*. 2003;58;903–910.
27. Magnico P. Hydrodynamic and transport properties of packed beds in small tude-to-sphere diameter ratio: pore scale simulation using an Eulerian and a Lagrangian approach. *Chem Eng Sci*. 2003;58;5005–5024.
28. Jullien R, Pavlovitch A, Meakin P. Random packings of sphere built with sequential model. *J Phys A: Math Nucl Gen*. 1992;25;4103–4113.
29. Mueller GE. Numerical simulation of packed beds with monosized spheres in cylindrical containers. *Powder Technol*. 1997;72;179–183.
30. Maier RS, Kroll DM, Bernard RS, Howington SE, Peters JF, Davis HT. Pore-scale simulation of dispersion *Phys. Fluids* 2000;12;2065–2079.
31. Succi S, Karlin IV, Chen H. Colloquium: Role of the H theorem in lattice Boltzmann hydrodynamic. *Rev Mod Phys*. 2002;74;1203–1220.
32. Ferziger JH, M. Peric M. *Computational Methods for Fluids Dynamics*. 3rd ed. Springer; 2002.
33. Hill RJ, Koch DL, Ladd AJC. Moderate-Reynolds-number flows in ordered and random arrays of spheres *J. Fluid Mech*. 2001;338;243–278.
34. Jolls KR, Hanratty TJ. Transition to turbulence for flow through a dumped bed of spheres. *Chem Eng Sci*. 1966;21;1185–1190.
35. Wegner TH, Karabelas AJ, Hanratty TJ. Visual studies of flow in a regular array of spheres. *Chem Eng Sci*. 1971;26;59–63.
36. Dybbs A, Edwards RV. *A new look at porous media fluid mechanics-Darcy to turbulent*. In: *Fundamentals of transport phenomena in porous media*. Bear J, Corapicioglu MY, eds. *NATO ASI Ser., Series E : Appl Sci*. 1984;82;201–258.
37. Rode S, Midoux N, Latifi MA, Storck A, Saatdjian E. Hydrodynamics of liquid flow in packed beds: an experimental study using electrochemical shear rate sensors. *Chem Eng Sci*. 1994;49;889–900.
38. Seguin D, Montillet A, Comiti J. Experimental characterization of flow regimes in various porous media -I: Limit of laminar flow regime. *Chem Eng Sci*. 1998;53;3751–3761.
39. Suekan T, Yokouchi Y, Hirai S Inertial flow structures in a simple-packed bed of spheres. *AIChE J*. 2003;49;10–17.
40. Rottschäfer K. Geschwindigkeitsverteilungen in durchströmten füllkörperschüttungen. München, Germany; 1996. PhD dissertation.
41. Ren X, Stapf S, Blümich B. NMR velocimetry of flow in model fixed-bed reactors of low aspect ratio. *AIChE J*. 2005;51;392–405.
42. Benenati RF, and Brosilow CB. Void fraction distribution in beds of spheres. *AIChE J*. 1962;8;359–361.
43. Dixon AG. The length effect on packed bed effective heat transfer parameters. *Chem Eng J*. 1985;31;163–173.
44. Li CH, Finlayson BA. Heat transfer in Packed beds - a reevaluation. *Chem Eng Sci*. 1977;32;1055–1066.
45. Tsang TH, Edgar TF, Hougen JO. Estimation of heat transfer parameter in a packed bed. *Chem Eng J*. 1976;11;57–66.
46. Yagi S, N. Wakao N. Heat and mass transfer from wall to fluid in packed beds. *AIChE J*. 1959;5;79–85.
47. Dixon AG. Thermal resistance models of packed bed effective heat transfer parameters *AIChE J*. 1985;31;826–834.
48. Freiwald MG, Paterson WR. Accuracy of model predictions and reliability of experimental data for heat transfer in packed beds. *Chem. Eng. Sci*. 1992;47;1545–1560.
49. Zehner P, Schlünder EU. Die effective Wärmeleitfähigkeit durchströmter Kugelschüttungen bei mäβigen und hohen temperature. *Chemie Ing Tech*. 1973;45;272–276.
50. Zehner P, Schlünder EU. Wärmeleitfähigkeit von Schüttungen bei mäβigen temperature. *Chemie Ing. Tech*. 1970;42;933–941.
51. Bauer R, Schlünder EU. Effective radial thermal conductivity of packings in gas flow. Part II. Thermal conductivity of the packing fraction without gas flow. *Int Chem Eng*. 1978;18;189–204.
52. Hennecke FW, Schlünder EU. Wärmeübergang in beheizten oder gekühlten Rohren mit Schüttungen aus Kugeln, Zylindern und Raschig-Ringen. *Chemie Ing. Tech*. 1973;45;277–284.
53. Martin H, Nilles M. Radiale Wärmeleitung in durchströmten schüttungsrohren. *Chem Eng Tech*. 1993;65;1468–1477.
54. Specchia V, Baldi G. Heat transfer in trickle-bed reactors. *Chem Eng Comm*. 1979;3;484–499.
55. Kunii D, Smith JM. Heat transfer characteristics of porous rocks. *AIChE J*. 1960;6;71–78.
56. Fahien RW, Smith JM. Mass transfer in packed beds. *AIChE J*. 1955;1;28–37.
57. Schwartz CE, Smith JM. Flow distribution in packed beds. *Ind Eng Chem*. 1953;45;1209–1218.
58. Morales M, Spinn CW, Smith JM. Velocities and effective thermal conductivities in packed beds. *Ind Eng Chem*. 1951;43;225–232.
59. Dorweiler VP, Fahien RW. Mass transfer at low flow rates in a packed column *AIChE J*. 1959;5;139–144.
60. Vortmeyer D, Schuster J. Evaluation of steady flow profiles in rectangular and circular packed beds by variational method. *Chem Eng Sci*. 1983;38;1691–1699.
61. Borkink JGH, Westerterp KR. Significance of the radial porosity profile for the description of heat transport in wall-cooled packed beds. *Chem Eng Sci*. 1994;49;863–876.
62. Schroeder KJ, Renz U, Elgeti K. *Forshungsberichte des landes Nordrhein-Westfalen*. Nr.3037 1981;43;2523–2532.
63. Mueller GE. Radial void fraction distributions in randomly packed fixed beds of uniformly sized spheres in cylindrical containers. *Powder Technol*. 1992;72;169–275.
64. Dixon AG. Wall and particle-shape effects on heat transfer in packed beds. *Chem Eng Comm*. 1988;71;217–237.
65. Dixon AG, Labua LA. Wall-to-fluid coefficient for fixed bed heat and mass transfer. *Int J Heat Mass Transfer*. 1985;28;879–881.
66. Melanson MM, Dixon AG. Solid conduction in low dt/dp beds of spheres, pellets and rings. *Int J Heat Mass Transfer*. 1985;28;383–394.
67. Dwivedi PN, Upadhyay SN. Particle-fluid mass transfer in fixed and fluidized beds. *Ind Eng Chem Process Des Dev*. 1977;16;157.
68. Argentano C, Bouvard D. Modeling the effective thermal conductivity of random packing of spheres through densification. *Int J Heat Mass transf*. 1996;39;1343–1350.
69. Cheng GJ, Yu AB, Zulli P. Evaluation of effective thermal conductivity from structure of a packed bed. *Chem Eng Sci*. 1999;54;4199–4209.
70. De Wash AP, and Froment GF. Heat transfer in packed beds. *Chem Eng Sci*. 1972;27;567–576.
71. Lerou JJ, Froment GF. Velocity temperature and conversion profiles in fixed bed catalytic reactors. *Chem Eng Sci*. 1977;32;853–861.
72. Dixon AG, Paterson WR, Cresswell DL. Heat transfer in packed beds of low tube/particle diameter ratio. *Am Chem Soc Symp Ser*. 1978;65;238–253.
73. Winterberg M, Tsotsas E, Modelling of heat transport in beds packed with spherical particles for various bed geometries and/or thermal boundary conditions. *Int J Therm Sci*. 2000;39;556–570.
74. Olbrich W, Potter O. Mass transfer from wall in small diameter packed beds. *Chem Eng Sci*. 1972;27;1733–1743.
75. Yagi S, Kunii D. Studies in heat transfer near wall surface in packed beds. *AIChE J*. 1960;6;97–104.
76. Winterberg M. and Tsotsas E, Impact of tube-to-particle-diameter ratio on pressure drop in packed beds. *AIChE J*. 2000;46;1084–1088.

Appendix

In the Winterberg model, the velocity field is computed with the Brinkman-Forchheimer equations (3) with the following expression of the porosity

$$\varepsilon(r) = 0.37\left(1 + 1.36\exp\left(-5\frac{R_t - r}{d_p}\right)\right) \qquad \text{(A1)}$$

and with the effective viscosity

$$\frac{\eta_{eff}}{\eta_f} = 2\exp\left(-0.002Re_p\right) \qquad \text{(A2)}$$

Figure A1 shows the radial profile of the axial velocity for the three Reynolds numbers used in this work with $d_t/d_p = 7.8$. The profile at $Re_p = 1$ and $d_t/d_p = 4$ is identical to the profile shown in.[76]

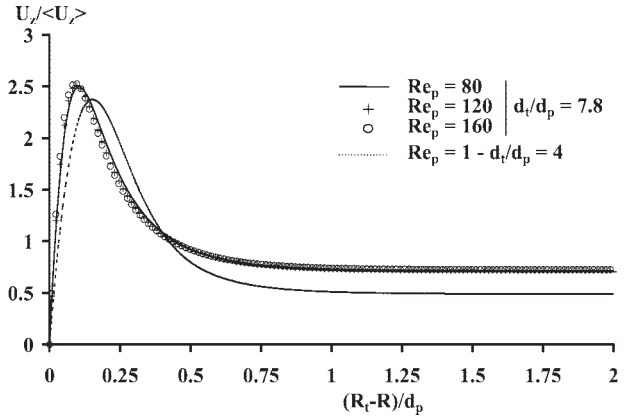

Figure A1. Radial profiles of velocity computed with the Brinkman-Forchheimer equation and the correlations of Winterberg.[7]

$d_t/d_p = 7.8$ and 4.

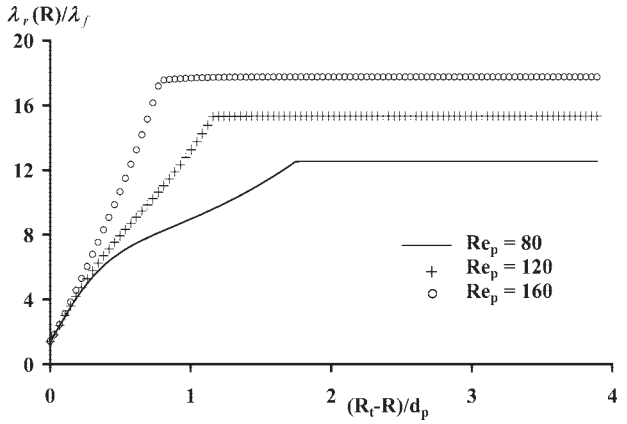

Figure A2. Radial profiles of thermal conductivity computed with the correlation of Winterberg.[7]

$d_t/d_p = 7.8$.

The temperature field is computed by solving the macroscopic heat balance equations with the local velocity field. The expression of the effective radial conductivity is

$$\lambda_r(r) = \lambda_{0r} + 0.125 Re_p Pr \frac{Ucore}{<U>} \left(\frac{R_t - r}{K_{2h} d_p}\right)^2 \lambda_f \quad \text{for } 0 < \left(\frac{R_t - r}{K_{2h} d_p}\right) < 1 \qquad \text{(A3a)}$$

$$\lambda_r(r) = \lambda_{0r} + 0.125 Re_p Pr \frac{Ucore}{<U>} \lambda_f \quad \text{for } 1 < \left(\frac{R_t - r}{K_{2h} d_p}\right) < \frac{R_t}{K_{2h} d_p} \qquad \text{(A3b)}$$

with $K_{2h} = 0.44 + 4\exp\left(-\frac{Re_p}{70}\right)$ and λ_{0r} computed with the correlation of Zehner.[49]

Figure A2 shows the radial profile of λ_r for the three Reynolds numbers used in this work and for $d_t/d_p = 7.8$.

The boundary conditions used in the computation are:

At the inlet: $Z = 0$, $T = T_{\text{inlet}}$ (r)

At the wall: $r = R_t$, $T = Tw$

At the outlet the temperature is extrapolated.

Manuscript received Sept. 11, 2007, revision received Sept. 5, 2008, and final revision received Dec. 12, 2008.